

# **Effervescent Atomization through Circular and Elliptical Nozzles**

Sana Shaghaghian

A Thesis  
in  
the Department  
of  
Mechanical, Industrial and Aerospace Engineering

Presented in Partial Fulfillment of the Requirements  
for the Degree of Master of Applied Science (Mechanical Engineering) at  
Concordia University  
Montreal, Quebec, Canada

March 2021

© Sana Shaghaghian, 2021

**CONCORDIA UNIVERSITY**  
**School of Graduate Studies**

This is to certify that the thesis prepared

By: Sana Shaghaghian

Entitled: Effervescent Atomization through Circular and Elliptical Nozzles

and submitted in partial fulfillment of the requirements for the degree of

**Master of Applied Science (Mechanical Engineering)**

complies with the regulations of the University and meets the accepted standards with respect to originality and quality.

Signed by the final Examining Committee:

Dr. Christian Moreau Chair

Dr. Fariborz Haghighat External Examiner

Dr. Christian Moreau Examiner

Dr. Ali Dolatabadi Supervisor

Approved by Dr. Martin D. Pugh  
Chair of Mechanical, Industrial and Aerospace Engineering Department

Dr. Mourad Debbabi  
Dean of Gina Cody School of Engineering and Computer Science

Date March 9, 2021

## ABSTRACT

### Effervescent Atomization through Circular and Elliptical Nozzles

Sana Shaghaghian

Effervescent atomization in quiescent air and in a subsonic crossflow are experimentally studied. The spray angle of an effervescent atomizer with an elliptical orifice is measured by employing the shadowgraph technique. Spray images were captured from both the minor and major axis views. The gas-liquid mass flow rate ratio (GLR) is in the range of 0.55 – 2.55 %. It is found that an increase in the aeration level results in an increase in the spray angle from both minor and major axis views. The results indicate that the spray angle from the minor axis view is wider than that from the major axis view and the difference increases as GLR rises.

Furthermore, the effervescent atomization in a gaseous crossflow is studied using circular and elliptical orifices with aspect ratios of 1, 3, and 0.3. Gas-liquid mass flow rate ratio varies between (0 – 7%) and liquid-air momentum flux ratio,  $q$ , is in the range of 2 – 23. The high-speed shadowgraph technique and image processing were utilized to visualize the spray trajectory and measure the spray penetration height. Moreover, an empirical correlation is developed as a function of GLR,  $q$ , aspect ratio and downstream location. Additionally, the laser diffraction technique is employed to analyze the spray droplet size distribution in a crossflow.

## **Acknowledgment**

I would like to express my gratitude and appreciation to my supervisor, Prof. Ali Dolatabadi, whose guidance and support during my graduate studies have been priceless. Without your endless support and attention, the completion of this research would not have been possible. Under your supervision, I have learned many valuable things in my research and my life, and I hope to continue learning from you in the future. Thank you for being an inspiration to me!

I would like to express my special thank to Dr. Mehdi Jadidi, whose exceptional capability and precious ideas has facilitated my research. Thank you for your valuable help in many aspects of my project. I have been fortunate to have your continuous support on this work!

I would like to thank Dr. Ali Akbarnozari, whose valuable collaboration on my experiments has accelerated my work. I am thankful to Mr. Rocco Portaro, Amir Jalini and Engineering Design and Manufacturing Lab (EDML) for their help in manufacturing the atomizer used in this project. I would like to recognize the Natural Science and Engineering Research Council of Canada (NSERC) and Concordia University for supporting this research financially.

I would appreciate my colleagues and friends in the Thermal Spray and Multiphase Flow Laboratory for all of their friendly supports. It has been a pleasure to be in the TSMF lab!

Also, to my dear friends, Mohammad, Shahrzad and Firoozeh, you should know that your friendship means a lot to me and your support and encouragement are priceless. Thank you for your listening ears. You are a treasure!

After all, no words can ever be found to express my unconditional love and appreciation to my parents! Thank you for always being there for me! I love you!

# Contents

List of Figures .....	vi
List of Tables.....	viii
Nomenclature.....	ix
<b>1 Introduction.....</b>	<b>1</b>
<b>1.1 Objective.....</b>	<b>8</b>
<b>1.2 Thesis Layout .....</b>	<b>9</b>
<b>2 Spray Structure of an Elliptical Effervescent Atomizer .....</b>	<b>10</b>
<b>2.1 Introduction .....</b>	<b>11</b>
<b>2.2 Experimental Setup .....</b>	<b>12</b>
2.2.1 Atomizer Geometry.....	12
2.2.2 Test Conditions .....	13
2.2.3 Spray Angle Measurement.....	14
<b>2.3 Results and Discussion .....</b>	<b>15</b>
<b>2.4 Conclusion .....</b>	<b>17</b>
<b>3 Aerated Circular and Elliptical Liquid Jets in a Gaseous Crossflow .....</b>	<b>18</b>
<b>3.1 Introduction .....</b>	<b>19</b>
<b>3.2 Experimental Methodology .....</b>	<b>21</b>
3.2.1 Test Setup.....	21
3.2.2 Test Conditions .....	25
3.2.3 Shadowgraph and Image Processing.....	26
3.2.4 Spray Droplet Size Analysis .....	29
<b>3.3 Results and Discussion .....</b>	<b>31</b>
3.3.1 Near-Field .....	31
3.3.1.1 Spray Visualization .....	31
3.3.1.2 Penetration Height.....	37
3.3.2 Far-field.....	42
3.3.2.1 Droplet Size Distribution.....	42
<b>3.4 Conclusion .....</b>	<b>49</b>
<b>4 Summary, Conclusions and Recommendations for Future Work .....</b>	<b>51</b>
<b>4.1 Summary and Conclusions .....</b>	<b>51</b>
<b>4.2 Future Work .....</b>	<b>53</b>
<b>Reference.....</b>	<b>54</b>
<b>Appendix .....</b>	<b>59</b>

## List of Figures

Figure 1.1 Example of a simple spray showing many features of typical atomization [1].	1
Figure 1.2 Common types of atomizers: a) Pressure atomizer, b) Rotary atomizer, c) Twin-fluid atomizer with internal mixing, and d) Twin-fluid atomizer with external mixing [3].	3
Figure 1.3 A typical effervescent atomizer [8].	5
Figure 1.4 Flow regimes in the discharge orifice of an effervescent atomizer [8].	6
Figure 2.1 Schematic of the effervescent atomizer (units are in mm).	12
Figure 2.2 Schematic of the experimental setup.	13
Figure 2.3 Spray angle measurement using the ImageJ software: a) thresholded image, b) average image after background subtraction.	15
Figure 2.4 spray at different GLRs: a) minor axis view, b) major axis view.	16
Figure 2.5 Effect of GLR on the spray angle from two imaging views.	16
Figure 3.1 Schematic of the wind tunnel and spray injection system.	22
Figure 3.2 The outside-in effervescent atomizer.	23
Figure 3.3 a) Circular orifice, b) Elliptical orifice.	24
Figure 3.4 Schematic of the elliptical and circular orifice aspect ratios.	24
Figure 3.5 Shadowgraphy setup.	27
Figure 3.6 Sample of shadowgraph images and image processing steps at $GLR = 7\%$ , $q = 4$ and $AR = 0.3$ .	28
Figure 3.7 Malvern Spraytec setup.	29
Figure 3.8 Measurement points for analyzing spray droplet size.	30
Figure 3.9 Shadowgraph images of non aerated liquid jet ( $GLR = 0$ ) in a gaseous crossflow.	33
Figure 3.10 Shadowgraph images of the aerated spray ( $GLR = 2\%$ ) in a gaseous crossflow.	34

Figure 3.11 Shadowgraph images of the aerated spray (GLR = 4%) in a gaseous crossflow.....	35
Figure 3.12 Shadowgraph images of the aerated spray (GLR = 7%) in a gaseous crossflow.....	36
Figure 3.13 Effect of aspect ratio on the spray trajectory at various $q$ and GLR. ....	40
Figure 3.14 Comparison of experimental data and predicted values by Eq. 1.....	41
Figure 3.15 Droplet size contour for different aspect ratios at GLR = 7% and $q = 4$ , the color map shows SMD (0 – 180 $\mu\text{m}$ ). ....	43
Figure 3.16 Droplet size contour for different aspect ratios at GLR = 4% and $q = 4$ , the color map shows SMD (0 – 220 $\mu\text{m}$ ). ....	44
Figure 3.17 Droplet size contour for different aspect ratios at GLR = 2% and $q = 4$ , the color map shows SMD (0 – 260 $\mu\text{m}$ ). ....	45
Figure 3.18 Weighted ensemble average of SMD versus downstream location for various GLRs and aspect ratios at $q = 4$ .....	46
Figure 3.19 Weighted ensemble average of SMD versus GLR at three downstream locations for various aspect ratios at $q = 4$ .....	46

## List of Tables

Table 2-1 Experiment conditions. ....	14
Table 3-1 Different flow rates in all test conditions.....	26
Table 3-2 Matrix of 48 experiments.....	26

## Nomenclature

$q$	Liquid to air momentum flux ratio ( $\rho_l u_l^2 / \rho_g u_g^2$ )
AR	Aspect ratio
$d$	Orifice diameter
$\rho$	Density
$u$	Velocity ( $m/s$ )
$D_{32}$	Sauter Mean Diameter (SMD)
GLR	Gas to liquid mass flow rate ratio ( $\dot{m}_g / \dot{m}_l$ )

### Subscripts:

$g$	gas
$l$	liquid

# 1 Introduction

Atomization is the transformation of bulk liquid into small droplets and dispersion of fine sprays occurs in many natural phenomena such as rain and waterfall mists. Importantly, sprays and atomization play an essential role in several industrial processes and automated applications, including agriculture, medicine, powder metallurgy, gas turbine engine and spray coating. Research in this field involves complex challenges due to the random nature of atomization. Figure 1.1 illustrates a typical spray with associated features. Some characteristics of a spray are: spray angle, liquid sheet, primary breakup, breakup length, drop formation, secondary breakup, drop size/velocity, volume flux distributions and droplet evaporation. These features are influenced by three general factors: a) the physical properties of the liquid, b) the internal design of the atomizer, c) the properties of the ambient air into which the spray is discharged.

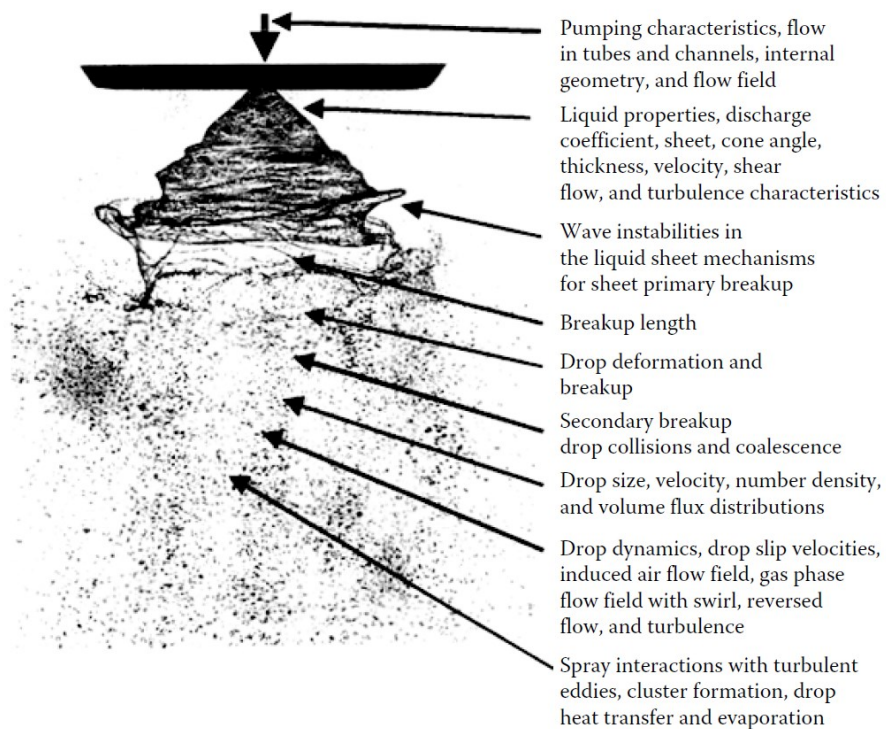


Figure 1.1 Example of a simple spray showing many features of typical atomization [1].

Liquid properties such as density, surface tension and viscosity strongly influence the spray characteristics and atomization. Some research shows that the effect of liquid density on the mean droplet size is relatively small [2]. Since the density of most liquids is slightly varied, the atomization performance is weakly affected by this property. On the other hand, surface tension plays an essential role in atomization. Generally speaking, surface tension is the resistance to forming a new liquid surface area. For example, a droplet is generated by a droplet generator when the gravity force exceeds the surface tension force [2]. Another important liquid property from many aspects is viscosity which may influence the drop size distribution, the spray pattern and the nozzle flow rate. An increase in viscosity causes a reduction in Reynolds. Therefore, it prevents the development of instabilities in the jet and delays liquid fragmentation and increases spray droplet size [2].

Different kinds of atomizers have been developed to produce sprays. It is necessary to know which kind of atomizer is suitable for a particular application based on the desired droplet size and velocity, spray shape, fluid properties, and operating conditions. Common types of atomizers used in various industries are categorized by means of the energy used for liquid disintegration. Energy sources can be the energy of the liquid itself (pressure), mechanical energy (rotation), external energy like gas (pneumatic), electrical and acoustic energies [3].

Pressure atomizers are the most common atomizer in technical applications. In pressure atomizers, a liquid discharges through a small orifice under high pressure, in which the pressure energy converts into velocity (kinetic energy). Pressure atomizers are typically used for liquids with low viscosity. Drawbacks of pressure atomizers are relatively large droplet sizes, low mass flowrates and the need to pressurize the liquid to rather high pressures [2], [3].

Rotary atomizers comprise a high-speed rotating surface that spreads the fed liquid radially

outward across its periphery. The rotating surface may be a smooth and flat disk or a slotted (vaned) wheel to direct the liquid to the periphery. In some rotary atomizers, a cup may be used instead of a disk. Contrary to pressure nozzles, rotary atomizers provide a variety of flowrates without the problem of nozzle blockage because the fluid is not flowing through tiny passages [3].

Twin-fluid atomizers (pneumatic atomizers) utilize the kinetic energy of pressurized gas that mixes with the liquid to generate spray. Gas and liquid in twin-fluid atomizers are mixed internally, inside the mixing chamber before the nozzle exit, or externally, outside of the nozzle. This type of atomizer, which can operate at low injection pressure and low flowrates, is used in several applications such as combustion, humidification, spray drying and thermal spray coating. Airblast and air-assist atomizers are examples of twin-fluid nozzles, which are mostly of the external mixing type. In Figure 1.2, common types of atomizers are shown.

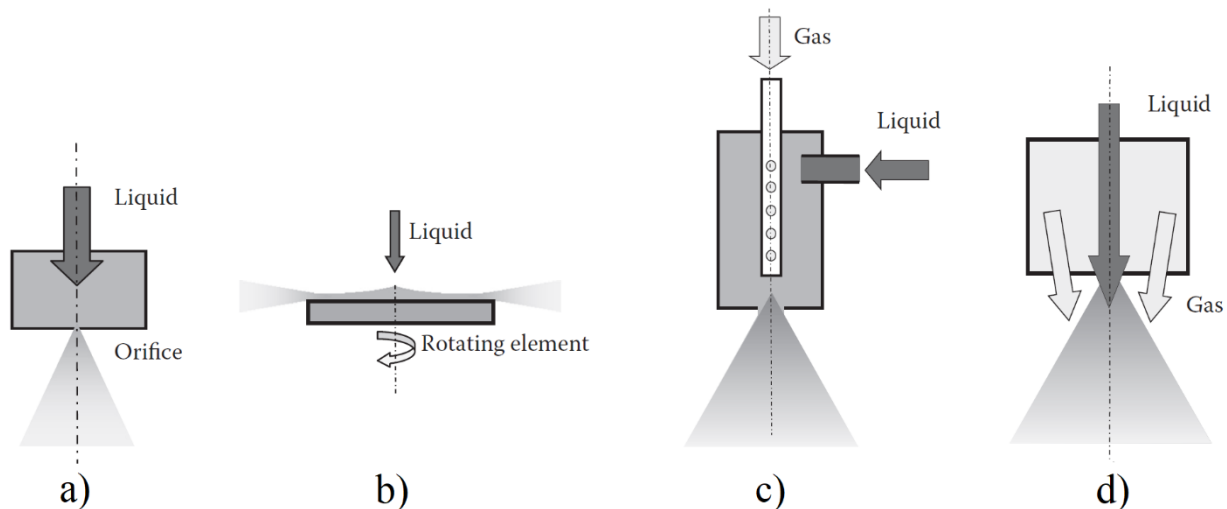


Figure 1.2 Common types of atomizers: a) Pressure atomizer, b) Rotary atomizer, c) Twin-fluid atomizer with internal mixing, and d) Twin-fluid atomizer with external mixing [3].

An effervescent atomizer is another example of twin-fluid nozzles that has an internal mixing system. Within effervescent atomizers, the aerating gas is injected into the liquid at a low velocity to form a bubbly flow upstream of the exit orifice. Lefebvre and co-workers developed the effervescent atomization technique in the late 1980s [4]–[7]. So far, several detailed studies have been conducted on effervescent atomization, which reveals the following advantages over other atomizers:

- Injection pressures can be several times lower than that of conventional pressure, rotary and twin-fluid atomizers [4], [6], [7].
- Effervescent atomizers generate smaller droplet sizes for any given injection pressure compared to more conventional atomization methods [4], [6], [7].
- High-quality atomization can be achieved at much lower gas flowrates than those in other types of twin-fluid atomizers [4], [6], [7].
- These atomizers can have considerably larger orifices than other nozzles preventing clogging problems and facilitating atomizer fabrication [5], [8]
- Effervescent atomization has better combustion efficiency due to the presence of aerating gas and produces lower pollutant emissions [4].
- Relatively, mean drop size is not affected by liquid viscosity; therefore, many fluids with a variety of viscosities can be atomized by a single atomizer [9]–[11].

The main disadvantage of effervescent atomizers is the necessity of a pressurized air supply. However, this may be relatively handled because the amounts of gas flow rate needed are small [8].

The main components of a typical effervescent atomizer are gas and liquid inlet ports, a mixing chamber and an exit orifice, which are shown in Figure 1.3. The gas and liquid are supplied

to the nozzle through inlet ports and mixed in the mixing chamber. Then the mixed bubbly fluid flows down to the exit orifice. The aerating gas supply pressure must be slightly higher than that of the liquid to penetrate the central perforated tube.

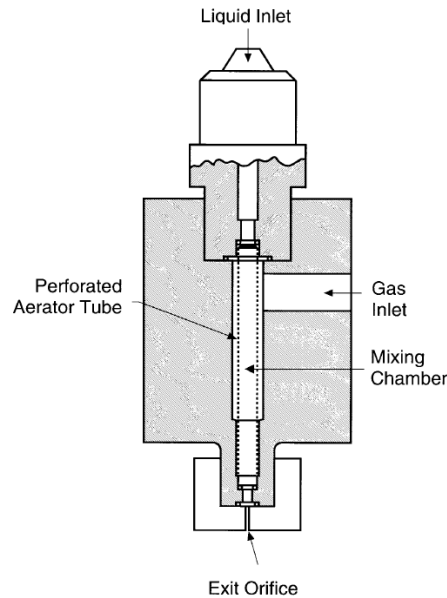


Figure 1.3 A typical effervescent atomizer [8].

There are two configurations for injecting aerating gas into the liquid inside effervescent atomizers; outside-in and inside-out gas injection system. In the outside-in gas injection system, the liquid flows inside an internal tube and the atomizing gas is injected into this tube through small holes on its wall. Many studies have been carried out on the outside-in gas injection system [6], [12]–[16]. In the other type, inside-out gas injection, the aerating gas which flows inside a perforated tube is injected into the surrounding liquid. A good number of studies have been focused on this type of gas injection system [4], [7], [10], [11], [17], [18].

The two-phase flow in the discharge orifice of an effervescent atomizer may include three regimes: bubbly flow, slug flow and annular flow, which are shown in Figure 1.4. In bubbly flow, the bubbles discharge from the orifice with the jet flow and experience a sudden pressure drop and expansion, which shatters the liquid into droplets. By increasing the GLR, the regime changes into

the slug flow, in which the expansion of gas slugs breaks up the liquid. By further increase in GLR, the annular regime is formed, in which the gas column is surrounded by an annular liquid film in the discharge orifice. Then, the gas core expansion breaks the liquid film into thin ligaments and droplets. The droplet sizes produced by the internal annular flow regime are smaller than those of bubbly flow and slug flow regimes. However, the main drawback of the annular flow is the necessity of a higher gas flow rate [8], [11], [19].

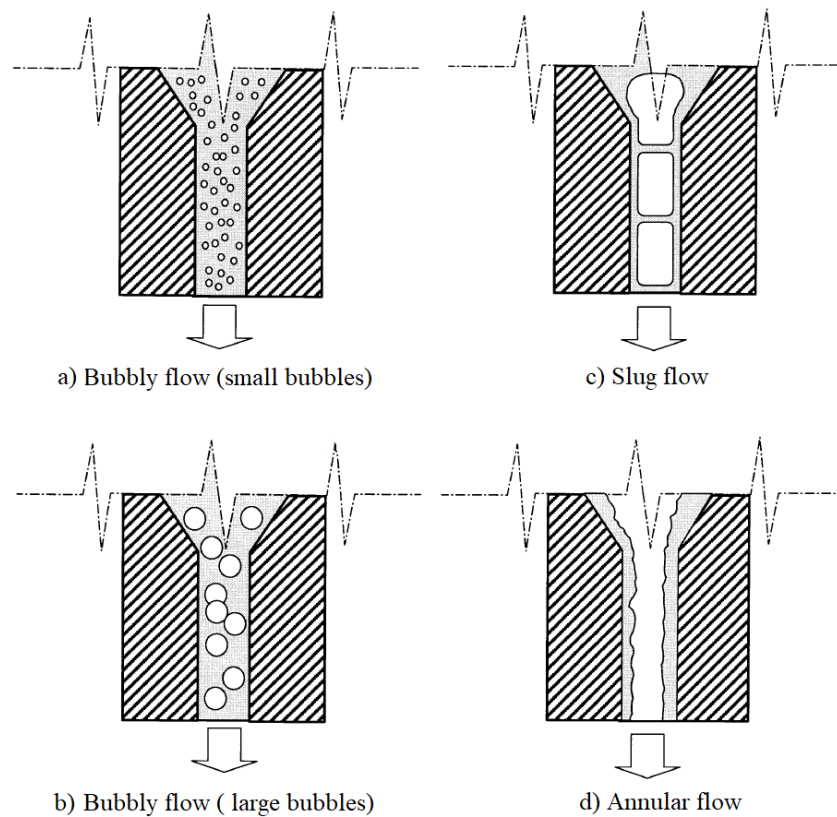


Figure 1.4 Flow regimes in the discharge orifice of an effervescent atomizer [8].

The internal geometry of an effervescent atomizer influences its performance and the quality of the spray. Mixing chamber dimensions, size/number/location of aeration holes, the length-diameter ratio of discharge orifice and the orifice shape/diameter are important geometrical parameters in an effervescent atomizer. Jedelsky et al. [20] and Mostafa et al. [21] stated that the mixing chamber length affects the radial distribution of droplet size and velocity. Sovani et al. [8]

and Chin et al. [22] concluded that a reduction in the length-diameter ratio ( $l/d$ ) results in the decrease of droplet sizes. Therefore, this geometrical parameter is considered an essential element in the internal design of an effervescent atomizer. Wang et al. [7] and Sovani et al. [8] showed that an aerator tube with multiple holes leads to a narrower droplet size distribution than an aerator tube with a single aeration hole. Several studies show that the effect of orifice diameter on the droplet size is negligible, indicating that the effervescent atomization is insensitive to this parameter [4]–[8].

In addition to the atomizer internal geometry, the shape of the discharge orifice influences the atomization remarkably. Among noncircular orifices, the elliptical orifice has attracted the attention of many researchers. Compared to a circular orifice, an elliptical orifice has shorter breakup lengths, which improves the performance of atomization [23]–[25]. In other words, as the free surface of a liquid jet always seeks patterns with minimum surface energy, elliptical jets require less energy to break up because of the inherent instabilities [26]. Moreover, the surface area of an elliptical jet is larger than that of a circular one with the same equivalent diameter; hence, it disintegrates faster, resulting in shorter breakup lengths [26].

In addition to the liquid properties and the atomizer type, the ambient condition where the spray is discharged affects the nature of atomization. Generally, there are two configurations for liquid atomization; in a quiescent air or a gaseous crossflow. A common fluid disintegration technique is injecting a liquid jet into a gaseous crossflow, which has many industrial applications, including gas turbine engines and thermal spray coating. The crossflow, which is perpendicular to the jet stream, causes instabilities on the liquid jet surface. Therefore, the column liquid undergoes deflection, starts to break into ligaments and primary atomization occurs. Then during the secondary atomization, large droplets entirely break up and disintegrate into smaller drops. Several

studies have been carried out on the characteristics of a liquid jet in crossflow atomization, such as penetration height, primary jet breakup, secondary breakup and droplet size distribution [27]–[33].

The nozzle type influences the liquid atomization in a gaseous crossflow, which distinguishes the atomization into two different categories: the jet in crossflow and the spray in crossflow. The aerated atomizers, such as effervescent nozzles, generate a spray in crossflow instead of a jet in crossflow. Only few studies have examined aerated atomization in a gaseous crossflow [34]–[38]. Seay et al. [39] measured the penetration height and the spray plume of a radial airblast nozzle in a subsonic crossflow. Tan et al. [40] experimentally studied the regimes of a twin-fluid jet in a gaseous crossflow using a dye-based shadowgraph technique. Another parameter that affects the atomization of liquid in a gaseous crossflow is the orifice shape. Recently, noncircular jets in crossflow has been investigated experimentally and numerically [26], [41]–[43].

## 1.1 Objective

As raised, many studies have been conducted on effervescent atomization and liquid jet in a gaseous crossflow. However, there is a knowledge gap, which is addressed here. The characteristics of effervescent atomization with an elliptical orifice have not been covered in the literature. This research aims at finding spray features from an effervescent atomizer with an elliptical orifice in still air and also gaseous crossflow.

The current study is carried out to cover the mentioned knowledge gap by answering the following questions:

- In quiescent air condition, how does the spray angle of an effervescent atomizer with an elliptical orifice vary from minor axis view to major axis view?
- How does the orifice shape influence the spray penetration height in a gaseous

crossflow in the near-field?

- How does the orifice shape influence the spray droplet size in a gaseous crossflow in the far-field?
- How liquid-air momentum flux ratio ( $q$ ), gas-liquid mass flow rate ratio (GLR) and aspect ratio (AR) affect the spray trajectory and droplet sizes in the crossflow?

## 1.2 Thesis Layout

This thesis is arranged in a manuscript-base, which consists of four chapters.

The first chapter introduces the overall concepts of atomization in quiescent air. The parameters that affected the spray quality, such as atomizer geometry and physical properties, are reviewed. Various common types of atomizers are introduced and compared together. Moreover, the effervescent atomization is explained. Finally, a brief description of the liquid jet in gaseous crossflow is presented and its characteristics, including penetration height, breakup and size distribution, are overviewed.

In chapter two, the spray structure of an effervescent atomizer with an elliptical orifice is investigated. The influence of gas-liquid mass flow rate ratio (GLR) on the spray angle is visually illustrated and calculated from the minor and major axis views.

In chapter three, effervescent atomization in a gaseous crossflow is experimentally studied. The effect of orifice shape, elliptical and circular, is examined on the jet trajectory and droplet size distribution. Furthermore, the spray penetration height is empirically calculated as a function of downstream location, GLR,  $q$  and AR.

Finally, in chapter four, summary and conclusions are presented following with some recommendations for future studies.

## 2 Spray Structure of an Elliptical Effervescent Atomizer

Sana Shaghaghian, Mehdi Jadidi, Ali Dolatabadi

Department of Mechanical, Industrial, and Aerospace Engineering, Concordia University,  
Montreal, QC, Canada, H3G 2W1

This paper has been published in the proceedings of the 5th World Congress on Momentum, Heat and Mass Transfer (MHMT'20), October 14 - 16, 2020, ~~Lisbon, Portugal~~ Virtual Conference and received the best paper award.

### **Abstract**

The spray structure of an effervescent atomizer with an elliptical orifice is studied using the high-speed shadowgraphy technique. The major to minor axis ratio of the ellipse is 3. The effect of gas to liquid ratios (GLR) in the range of 0.55 – 2.55 % on the spray angle is analyzed. The water flow rate was constant for all the tests, while the airflow rate varied. Two imaging views of minor and major axes were captured for each test condition. This study shows that an increase in the gas flowrate results in an increase in the spray angle from both imaging views. It was shown that the spray angle from the minor view is wider than that of the major view, and the difference magnifies by increasing the GLR.

**Keywords:** Elliptical effervescent atomizer, outside-in gas injection, two-phase flow, spray angle, gas to liquid ratio, high-speed imaging.

## 2.1 Introduction

An effervescent atomizer, which can be categorized as twin-fluid atomizers, mixes two phases of gas and liquid internally. The atomizing gas is injected into the flowing liquid at a low velocity to create a mixture of bubbly two-phase flow in the mixing chamber before the nozzle exit [8]. Numerical simulation provides an understanding of the internal and external flows in this kind of nozzles [44]. Effervescent atomizers have been used in various engineering applications, such as internal combustion engines, gas turbine combustors, pharmaceutical processes, agricultural sprays, and thermal spray coatings, where pure liquid or complex fluids should be fragmented into small droplets.

Spray angle, which demonstrates the coverage region of the spray, is one of the essential characteristics of atomization influencing the performance of a nozzle. In general, the atomizer type and its dimensions, ambient air pressure, and liquid properties influence the spray angle. Chen and Lefebvre [16] investigated the effect of liquid properties and ambient pressure on the spray angle of the effervescent atomizer. They observed that for ambient pressures below 0.5 MPa, a continuous increase in gas to liquid mass ratio causes the spray angle to rise to a maximum value and then gradually decreases. While at high ambient air pressures, an increase in GLR causes a slight rise in the spray angle. In addition, they showed that lower viscosity and surface tension results an increase in spray angle. Other studies showed that when GLR increases, the spray angle widens because a higher amount of energy exists for aeration gas as it leaves the nozzle orifice [45], [46].

Using noncircular nozzles can be effective due to their improved atomization performance and shorter breakup length [25]. It has been recently demonstrated that the spray angle in an elliptical nozzle is larger than that in a circular nozzle [47].

In the present study, the spray angle of an effervescent nozzle with an elliptical orifice is investigated at various GLRs and constant ambient air pressure. The shadowgraph images were used to measure the spray angle with an image processing technique. For each test condition, two different views of the elliptical nozzle are considered.

## 2.2 Experimental Setup

### 2.2.1 Atomizer Geometry

The effervescent nozzle used in this study has an outside-in gas injection configuration, which provides a large liquid flow area to prevent clogging when the nozzle is used for complex fluids such as suspensions [20]. This configuration has been frequently used in previous studies [48]–[50]. In this design, the liquid flows through an internal tube, and the aeration gas, which flows around the central tube, is injected into the liquid by some small holes on the inner tube. Figure 2.1 shows the schematic of this nozzle. 24 aeration holes with a 1 mm diameter are used to inject gas into the mixing chamber. The exit orifice has an elliptical shape with the major, minor, and equivalent diameter of 2.03, 0.67, and 1.16 mm, respectively.

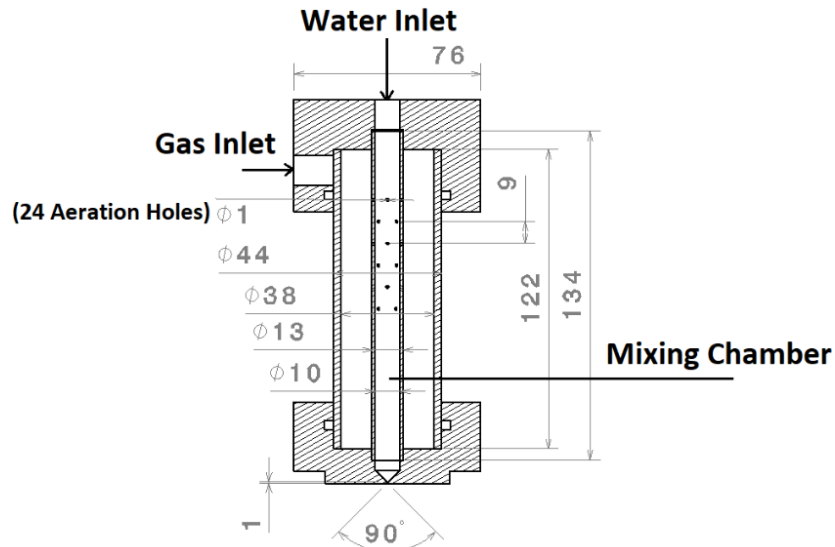


Figure 2.1 Schematic of the effervescent atomizer (units are in mm).

## 2.2.2 Test Conditions

Figure 2.2 shows the schematic of the experimental setup, which consists of a liquid pressure vessel, water flowmeter, gas flowmeter, air supply system, effervescent atomizer, high-speed camera, and light source. Distilled water is used as the test liquid. A high-speed camera (Photron S A1.1) with 3  $\mu$ sec shutter speed and 5000 frames per second with a resolution of  $1024 \times 1024$  pixels and a lens (AF Micro-Nikkor 105 mm f/2.8) are used to record the images from two sides of the spray, major and minor axis views. For the backlight, an LED light (120 W, Schott, California USA) is utilized. The water flowrate is kept constant at 397 mL/min and the gas flow rate varies from approximately 2000 to 8500 mL/min. The pressures of the water tank and pressurized air are set to 0.35 MPa. Table 2-1 demonstrates the 8 test conditions. The distance between the spray and the camera lens was kept at 15 cm.

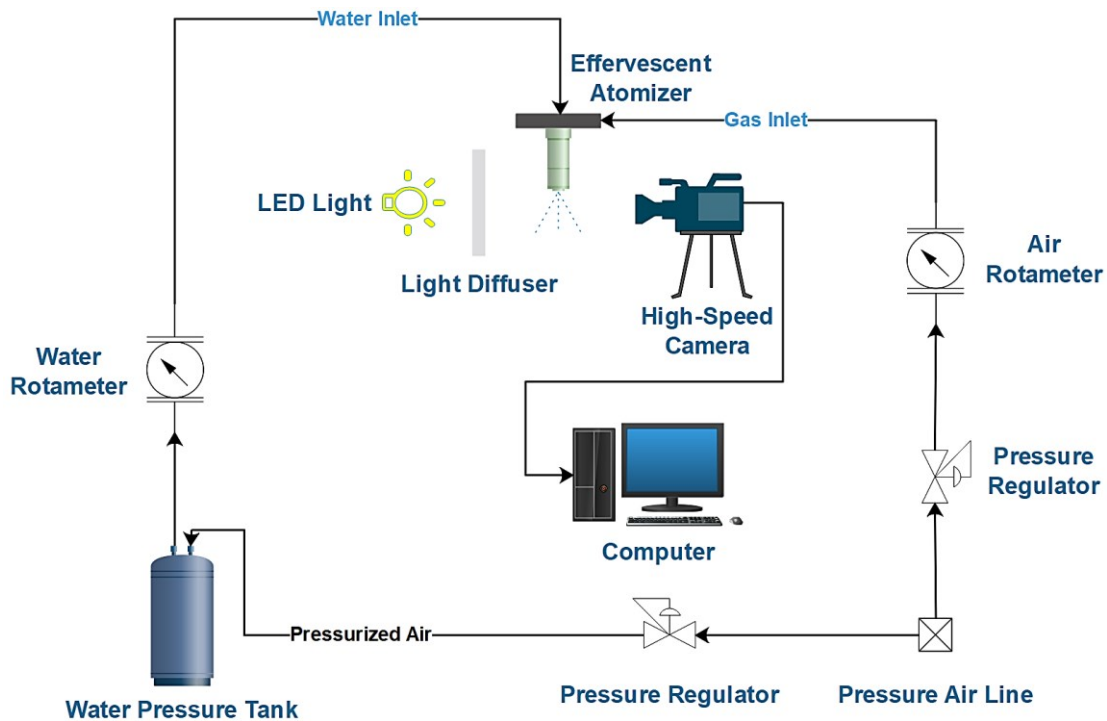


Figure 2.2 Schematic of the experimental setup.

Table 2-1 Experiment conditions.

Test number	Water flowrate (mL/min)	Gas flowrate (mL/min)	GLR %	Imaging view (axis)
1	397	1780	0.54	Minor
2	397	4125	1.25	Minor
3	397	6275	1.90	Minor
4	397	8423	2.55	Minor
5	397	1780	0.54	Major
6	397	4125	1.25	Major
7	397	6275	1.90	Major
8	397	8423	2.55	Major

### 2.2.3 Spray Angle Measurement

For each test, 5000 frames were recorded to calculate the spray angle at 10 mm from the nozzle exit. Moreover, 1000 frames were captured without the spray as the background images. The spray angle was measured on the average image, wherein each pixel contains the average intensity of all frames. To reduce the effect of spray fluctuation and have an unchangeable spray domain, a minimum of 800 images are required for getting an average image of spray independent from the number of frames. By using the ImageJ software, the average background image was subtracted from the average spray image. Then a threshold of 90% was applied to determine the spray edge on the resultant image. This threshold value has been used in other studies [38], [51]. A tangent line drawn to the spray periphery determines the spray radius,  $R2$  (in mm), at the stand-off distance of 10 mm. At each imaging view,  $R1$  (in mm) is the orifice radius (major or minor axis). The angle between the tangent line and the vertical line, which connects the orifice exit to  $R2$ , shows the spray half-angle ( $= \tan^{-1}((R2 - R1)/10)$ ). Figure 2.3 demonstrates the average image and the thresholded image for test number 5.

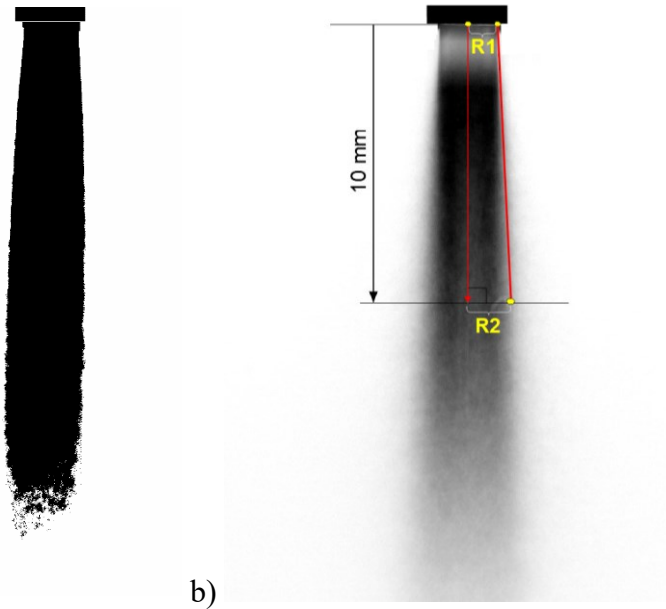


Figure 2.3 Spray angle measurement using the ImageJ software: a) thresholded image, b) average image after background subtraction.

## 2.3 Results and Discussion

Figure 2.4 shows the spray angle variations of the minor and major views at different GLRs. It can be seen that an increase in the gas flowrate (i.e., increase in GLR) causes a rise in the spray angle for both major and minor views. It is evident that as the amount of gas flow rate increases, the energy of atomizing gas gets larger to burst bubbles when they go through the nozzle exit. As a result, the aerating gas atomizes water in the broader area with a larger spray angle. The other parameter which affects the spray angle is the orifice shape and its diameter. At a particular GLR, the spray angle is broader from the minor axis view compared to the major axis view, which is apparent in Figure 2.5. Another intriguing conclusion that can be made from this figure is that as the amount of GLR increases, the difference between the spray angle of major and minor views increases. The smaller diameter of the exit orifice in the minor axis causes a wider spray due to the stronger air bubble bursting.

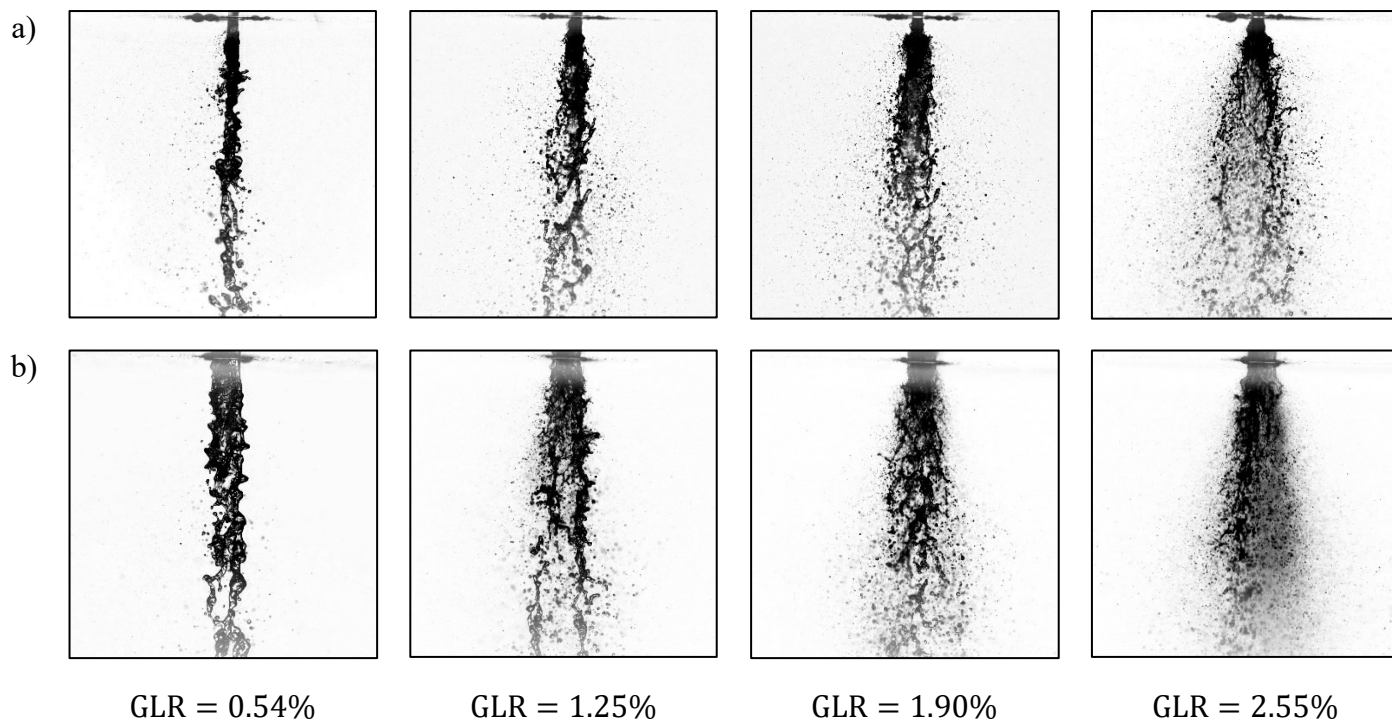


Figure 2.4 spray at different GLRs: a) minor axis view, b) major axis view.

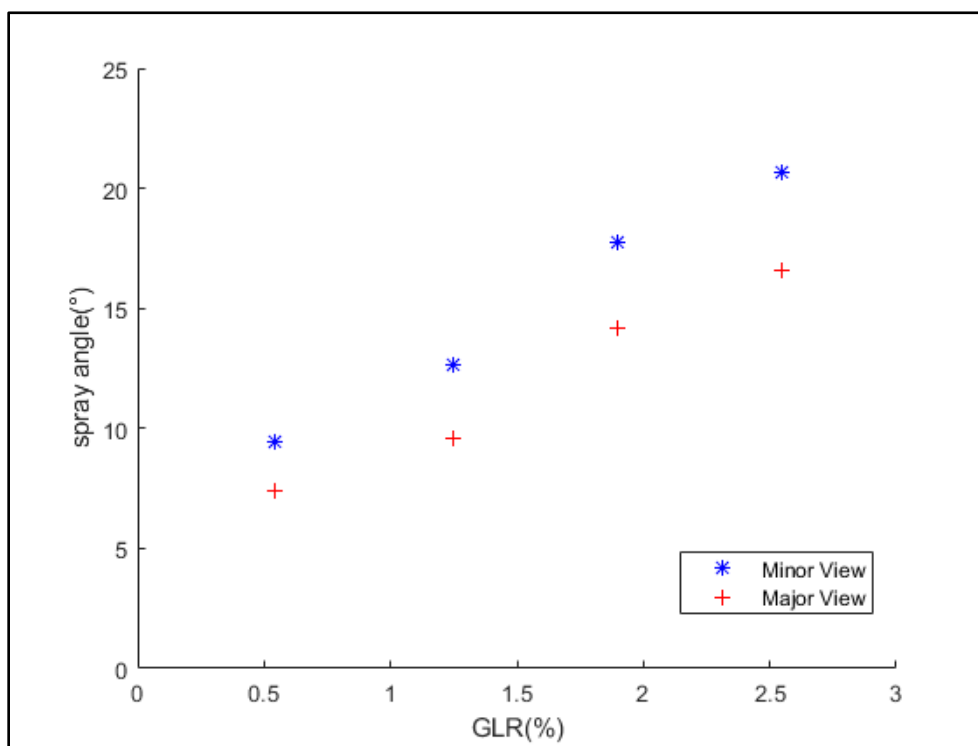


Figure 2.5 Effect of GLR on the spray angle from two imaging views.

## 2.4 Conclusion

Spray angle is experimentally investigated using high-speed shadowgraph technique for an elliptical effervescent atomizer. For each test case, the average image, which is the superimposition of 800 frames, is used to measure the average spray angle. The effect of GLR on the spray angle from the two minor and major axis views is studied. It is found that the spray has a wider angle from the minor view in comparison with the major view. The reason is that the smaller diameter of the orifice from the minor view increases the strength of bubble bursting, which splashes water in a broader domain. Furthermore, the energy of aerating gas depends on the amount of air that exists for the atomization of water. As the GLR increases with a rise in the gas flowrate, the spray angle will increase; for example, the spray angle at a GLR of 0.5% is approximately 8 degrees, which rises to 20 degrees at the higher GLR of 2.55%.

### 3 Aerated Circular and Elliptical Liquid Jets in a Gaseous Crossflow

Sana Shaghaghian, Mehdi Jadidi, Ali Akbarnozari, Ali Dolatabadi

Department of Mechanical, Industrial, and Aerospace Engineering, Concordia University,  
Montreal, QC, Canada, H3G 2W1

This article will be submitted to the journal of Experiments in Fluids.

#### **Abstract**

In this study, the atomization of an effervescent atomizer with an elliptical and circular orifice is investigated experimentally in the gaseous crossflow. The shadowgraph technique has been used to visualize the near field of the spray atomization. Image processing has been performed on the shadowgraph images to measure the spray penetration height in crossflow. Moreover, an empirical correlation for the spray penetration height has been developed as a function of gas-liquid mass flowrate ratio, liquid-air momentum flux ratio, orifice aspect ratio and downstream location. The laser diffraction technique has been used to analyze particle size of the aerated elliptical and aerated circular jets in a gaseous crossflow. For each orifice shape, the effect of gas-liquid ratio and downstream location on the Sauter Mean Diameter has been studied. The results have been shown that the aerated circular jet penetrates higher into the gaseous crossflow than the aerated elliptical jet. Besides, the aerated circular jet in crossflow mainly generates smaller drop sizes compared to the aerated elliptical jet.

**Keywords:** Effervescent atomizer, elliptical orifice, liquid jet in crossflow, highspeed imaging, penetration height, Sauter Mean Diameter.

### 3.1 Introduction

An effervescent atomizer is kind of a twin fluid atomizer that mixes air and liquid internally. Effervescent nozzles generate fine sprays with the help of aerating gas compared to other types of atomizers. Atomization of liquids plays an essential role in many applications, including thermal spraying processes, gas turbines, agricultural sprays, paint sprays and fire suppressions. Many studies have been carried out to investigate the influence of atomizing gas, gas-liquid mass flow rate ratio (GLR), air injection geometry and exit orifice geometry on the effervescent atomization (Lund et al. [52]; Lefebvre et al. [4]; Petersen et al. [18]; Li et al. [53]).

Aerated circular liquid jets in gaseous crossflows have been studied extensively. Lin et al. [34], [51] experimentally studied the aerated liquid jets injected into gaseous crossflows using PDPA and pulsed shadowgraphy. In general, it was shown that aerated liquid jets are able to produce densely fine droplets within a relatively short distance after injection. Droplet size decreases as the Mach number and GLR increase, but it does not significantly depend on the liquid-air momentum flux ratio ( $q$ ). It was found that the spray cross-sectional area and the penetration height increase with a rise of  $q$ , GLR and downstream location. In other words, the penetration height for an aerated liquid jet is greater than that of a pure liquid (i.e., nonaerated) jet under the same crossflow and liquid flow conditions. Moreover, they developed a correlation to estimate the penetration height of aerated circular liquid jets in subsonic crossflows. Miller et al. [35] studied the breakup of an aerated circular liquid jet experimentally in subsonic gaseous crossflow. Their measurements were performed at the near-injector dense-spray region ( $x/d < 50$ ). The droplet sizes and locations were measured by 3-D microscopic digital holography. Their results showed a reduction in droplet sizes with downstream distance as a result of the secondary breakup. Lee et al. [36], Sallam et al. [54], and Olinger et al. [37] worked on digital holographic technique for more

accurate measurement of droplet size, velocity and sphericity at the near field of aerated liquid jets in crossflow. Their results revealed that the Sauter mean diameter (SMD) is inversely proportional to  $(x/d)$  and GLR. Saleh et al. [38] investigated the penetration of aerated suspension jets in crossflows at different GLR and  $q$ . Various types of suspended solid particles with different concentrations were examined. The penetration height was measured by the shadowgraphy technique. They developed two correlations to predict the penetration height for nonaerated and aerated jets.

The elliptical liquid jet in gaseous crossflows has been studied recently. Morad et al. [55] experimentally studied trajectory and penetration of elliptical liquid jets in a gaseous crossflow at various liquid-air momentum flux ratios between 1-300. High-speed imaging was used to obtain windward jet trajectories for two aspect ratios. They proposed an empirical correlation to show the penetration height. Yoonho et al. [56] studied elliptical liquid jet trajectories in subsonic crossflows experimentally. One circular orifice and four elliptical orifices with aspect ratios varied from  $1/3$  to 3 were examined. Aspect ratio is defined as the ratio of the diameter perpendicular to the crossflow to the diameter in the crossflow direction. The injection pressure drop was changed between 1 – 6 bar and the liquid-air momentum flux ratio was from 15 to 106. The upper boundary and centerline of the liquid jets were detected on backlit spray photographs. They proposed an empirical equation of liquid jet trajectory for circular and elliptical liquid jets. They showed that their empirical correlation for the circular jet could be employed for the elliptical liquid jets with aspect ratios smaller than one. Jadidi et al. [43] studied the breakup and penetration of elliptical liquid jets in a subsonic gaseous crossflow by utilizing the shadowgraph technique. The gas Weber number was less than 15, the liquid-gas momentum flux ratio ( $q$ ) and the orifice aspect ratio (AR) were 50 – 320 and 0.22 – 4.47, respectively. Jet penetration height was considerably affected by

the momentum flux ratio and the orifice aspect ratio. Their results showed that circular liquid jets penetrate more than elliptical jets at a fixed  $q$ . However, the penetration of elliptical jets with  $AR < 1$  is slightly less compared to circular jets. They developed empirical equations for the jet penetration height and the column breakup location of elliptical and circular orifices. Farvardin et al. [41] numerically simulated the breakup, droplet size and penetration height of elliptical and circular jets in gaseous crossflows. They showed that as the aspect ratio increased, the jet penetration in crossflow decreased.

In the current study, spray atomization of an effervescent atomizer with elliptical and circular orifices in a gaseous crossflow is investigated. The near-field as well as far-field are examined experimentally. The high-speed spray images are illustrated for both elliptical and circular aerated and non-aerated jets at different liquid-air momentum flux ratios. An empirical equation is proposed for jet penetration heights as a function of various process parameters. Furthermore, droplet sizes of the spray in a crossflow are measured and the Sauter Mean Diameter (SMD) is calculated for elliptical and circular aerated jets in crossflow.

## **3.2 Experimental Methodology**

### **3.2.1 Test Setup**

The experimental tests were performed in an open-loop subsonic wind tunnel with a square cross test section of  $100 \times 100$  mm and a length of 750 mm. The test section is made of clear acrylic for flow visualization and imaging purposes. The blower fan connected to the wind tunnel can control the air velocity inside the test section up to 45 m/s. The PIV characterization of air velocity inside the test section was performed with a very fine spray reported by Farvardin et al. [30]. Their PIV tests showed that the air velocity is constant and parallel inside the test section

except for the thin boundary layers on the wall, which is smaller than 10 mm. They also reported that the turbulence intensity of 9% exists upstream of the injection location. In the current study, to measure and calibrate the air velocity in the test section, a Pitot tube is used.

As shown in Figure 3.1, the spray injection system consists of a liquid pressure tank, water rotameter, gas rotameter, pressure regulator, air supply, and an effervescent atomizer. The nozzle is installed on the upper mid-plane of the test section with a 200 mm axial distance from the inlet plane. The nozzle exit is set flush with the inner surface of the test section. Figure 3.1 shows the schematic of the spray injection system and the test section of the wind tunnel. One line of the air supply pressurizes the water inside the stainless-steel liquid vessel in which the pressure regulator controls its pressure. The other line of the pressurized air supplies the effervescent nozzle with the aerating gas after passing through the pressure regulator. Two rotameters are used to control water flowrate and aeration gas flowrate going into the atomizer.

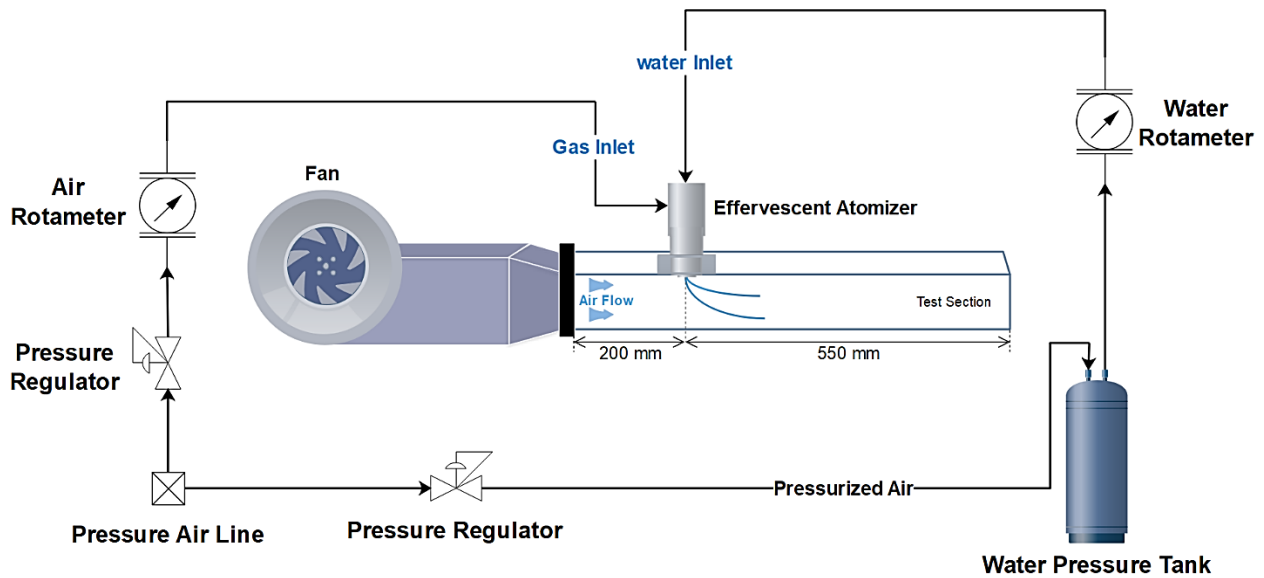


Figure 3.1 Schematic of the wind tunnel and spray injection system.

The current nozzle shown in Figure 3.2 is an outside-in effervescent atomizer used in our previous study [57]. The liquid flows inside a perforated tube and the aeration gas flows around

this tube, which penetrates the liquid from the holes on this tube. Hence, the pressure of aerating gas must be slightly more than the pressure of the liquid. The number of aeration holes on the inner tube is 24, with a diameter of 1 mm. It has been shown that an aerator tube with multiple holes results in a narrower droplet size distribution than an aerator tube with a single aeration hole [7], [8]. Two pieces are designed as the bottom part, one has a circular orifice and the other has an elliptical orifice. The diameter of the circular orifice is 0.94 mm. The major, minor and equivalent diameters of the elliptical orifice are 2.03 mm, 0.67 mm and 1.16 mm, respectively. Figure 3.3 shows the circular and elliptical orifices.

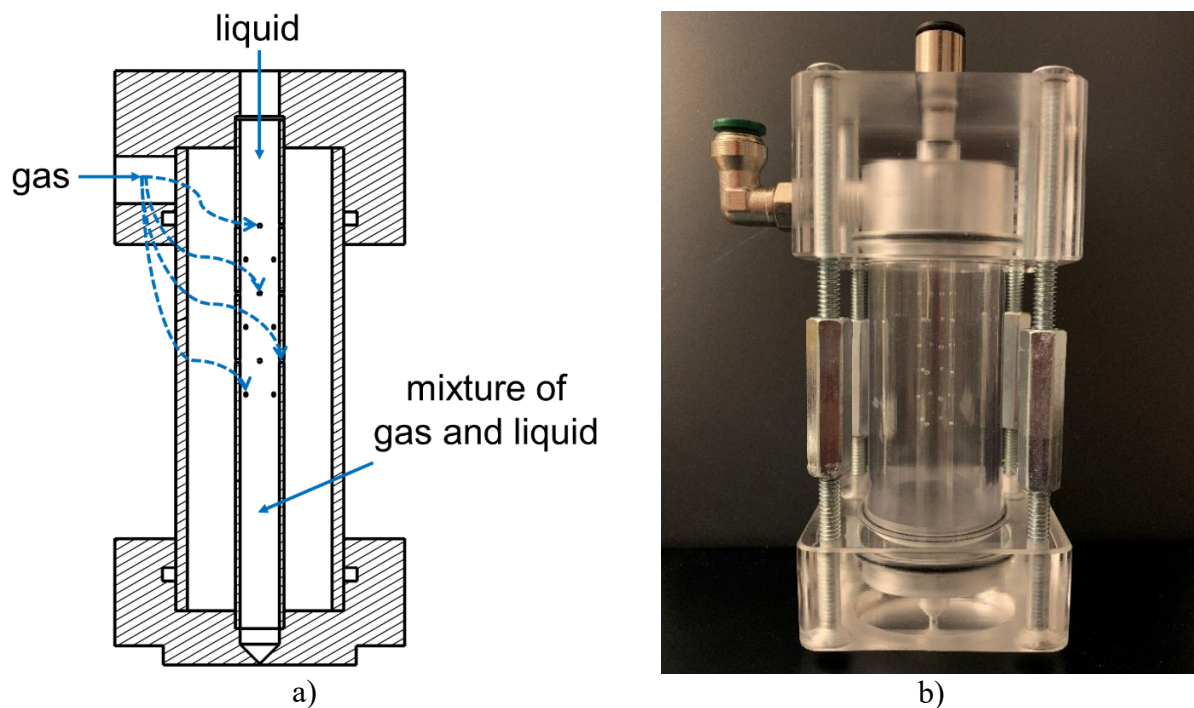


Figure 3.2 The outside-in effervescent atomizer.

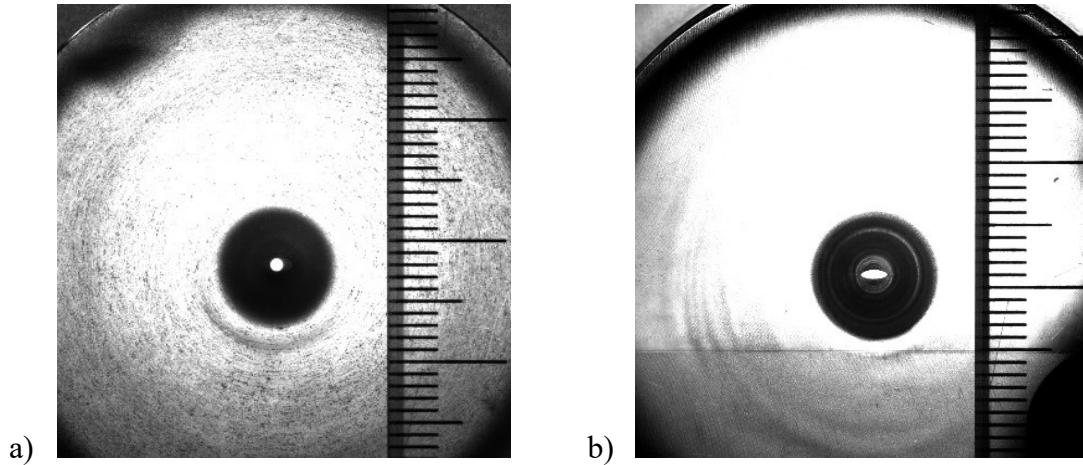


Figure 3.3 a) Circular orifice, b) Elliptical orifice.

In this study, the aspect ratio (AR) is defined as the ratio of the diameter perpendicular to the crossflow to the diameter in the crossflow direction [41], [43], [56]. The elliptical orifice aspect ratios are 3.03 and 0.33, and the circular orifice aspect ratio is 1. Figure 3.4 demonstrates the definition of the aspect ratio.

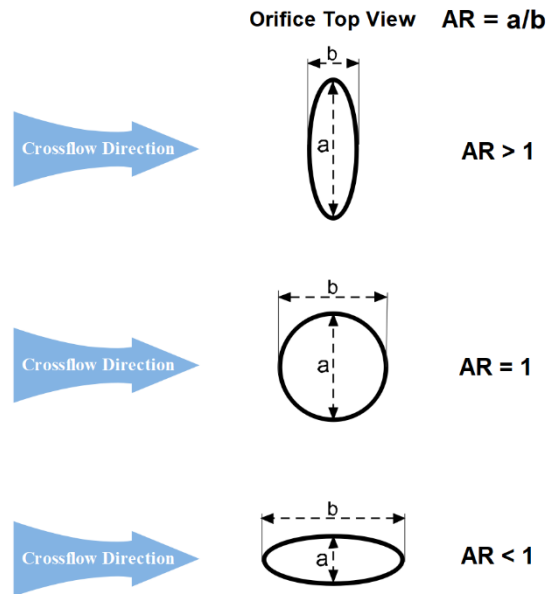


Figure 3.4 Schematic of the elliptical and circular orifice aspect ratios.

### 3.2.2 Test Conditions

Distilled water is used as the test liquid and the air is used as the aerating gas to make the sprays in the gaseous crossflow. In order to compare the circular nozzle atomization in crossflow with the elliptical one, dimensionless numbers such as gas to liquid ratio (GLR), aspect ratio (AR), Weber ( $We$ ) and momentum flux ratio ( $q$ ) are used. To have different values for  $q$ , the wind tunnel velocity is varied while the injection water velocity is kept constant. The liquid injection velocity is calculated as the water volume flowrate over the atomizer orifice area, which has been used in the literature [38]. By adding the atomizing gas to the nozzle, the liquid film area in the orifice and consequently the effective momentum flux ratio is changed. However for simplicity, the value of  $q$  is calculated based on the non-aerated liquid jet condition. Hence, to show the effect of the atomizing gas, GLR is calculated and considered for aerated liquid jets. The liquid and the aerating gas volume flowrates are measured by two different rotameters. To generate different GLRs, the aerating gas volume flowrate changes while the liquid volume flowrate is kept constant. Table 3-1 summarizes the flow rates of gas and liquid at various aeration levels. All experiments are performed at atmospheric pressure (101.32 kPa) and room temperature (22°C). The pressure of the water tank and the aerating gas is kept constant at 0.21 MPa. Atomization in a gaseous crossflow is examined for three aspect ratios ( $AR = 0.3, 1, 3$ ) at four different GLRs (0 – 7%) for four different  $q$  (2 – 23), which generates a matrix of sixteen experiments for each aspect ratio. Table 3-2 demonstrates all 48 experiments.

Table 3-1 Different flow rates in all test conditions.

Orifice Shape	Elliptical ( $d_{\text{equivalent}} = 1.16 \text{ mm}$ )				Circular ( $d = 0.94 \text{ mm}$ )			
Gas-liquid ratio, GLR (%)	0	2	4	7	0	2	4	7
Aerating gas flowrate (mL/min)	No Air	2825	5866	9070	No Air	1842	3829	5910
Water flowrate (mL/min)	158	158	158	158	103	103	103	103

Table 3-2 Matrix of 48 experiments.

<b>AR</b>	<b>GLR (%)</b>	<b><math>q</math></b>
0.3, 1, 3	0, 2, 4, 7	2, 4, 8, 23

### 3.2.3 Shadowgraph and Image Processing

High-speed imaging and image processing are used to reveal important details of fluid behaviour. Photron SA1.1 high-speed camera with a resolution of  $1024 \times 1024$  pixels and a Nikon lens (AF Micro Nikkor 105mm 1:2.8) was used to record the side-view images of the spray inside the wind tunnel. The shutter speed and framerates were set to  $1\mu\text{s}$  and 5000 frames per second, respectively. An LED light (150 W, GS Vitec Multiled QT) was used as the backlight. In order to have a homogeneous background, a vellum paper was installed in front of the LED light to diffuse illumination.

Figure 3.5 shows the shadowgraph system. The captured images are saved to the computer connected to the camera via the Photron FASTCAM Viewer (PFV) software.

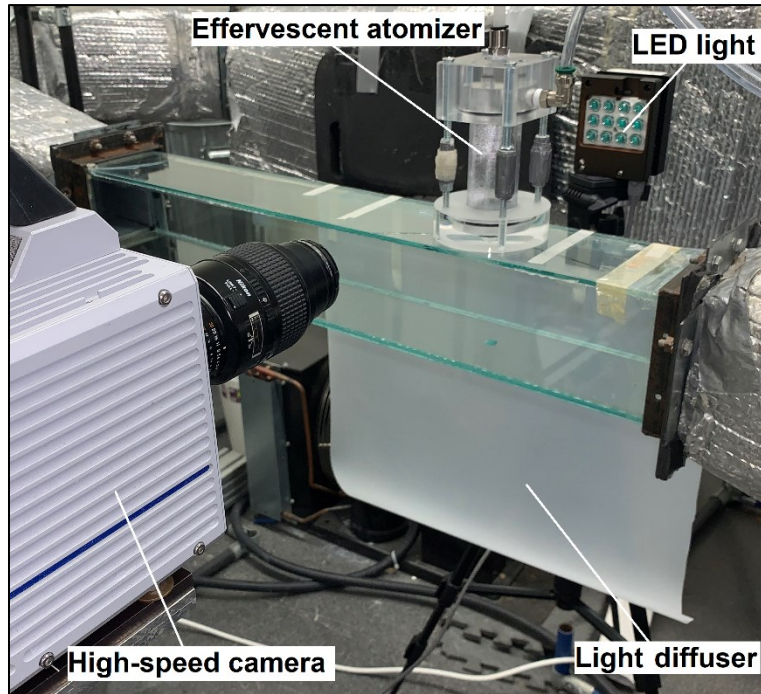
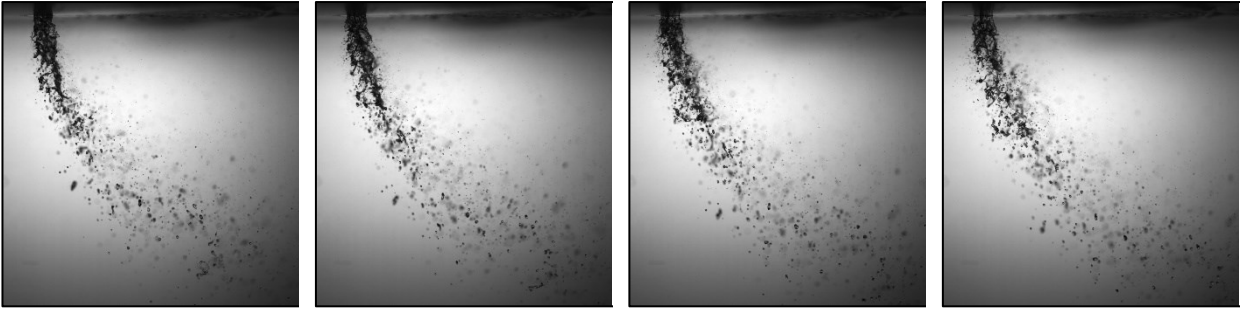


Figure 3.5 Shadowgraphy setup.

For each experiment, a set of 5000 frames of the spray in crossflow are recorded and superimposed to get an average spray image. Furthermore, a set of 100 frames without any spray are captured and averaged as a background image. Then, the averaged background image is subtracted from the averaged spray image [38]. A threshold of 90% is applied to the resultant image to detect the spray boundary and formulate the penetration height. Thresholding, which is selected based on similar studies [38], [51], reduces the noises of the average image and increases the accuracy of boundary detection. A series of points were placed manually along the spray's windward boundary for obtaining the spray trajectory. The line connecting these points represents the windward side of the spray. The image processing was done by ImageJ software [58].

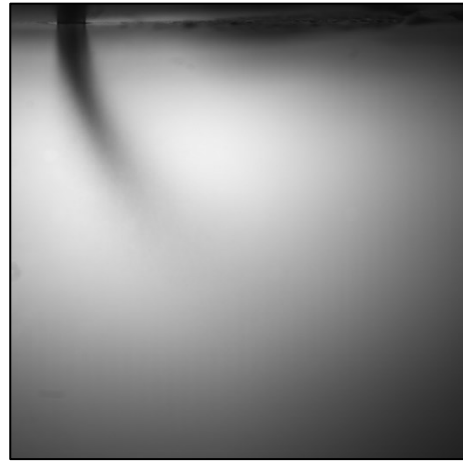
Figure 3.6 shows four consecutive frames as an example of the spray and image processing steps applied to the images sequentially, which is related to the case of  $GLR = 7\%$ ,  $q = 4$  and  $AR = 0.3$ .



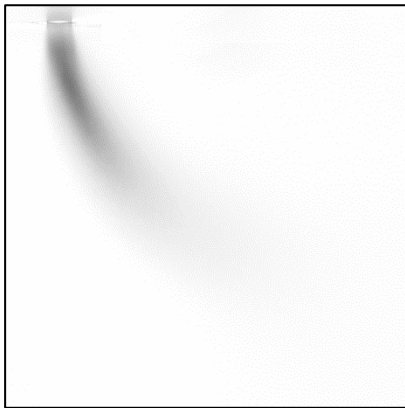
a) Four consecutive images of the spray



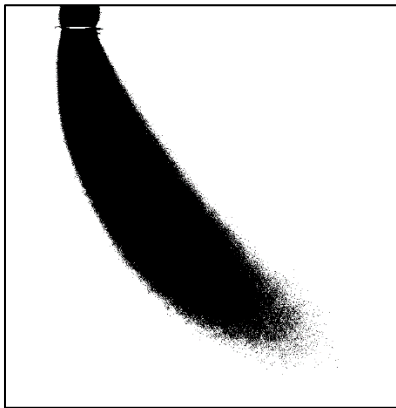
b) Averaged background image



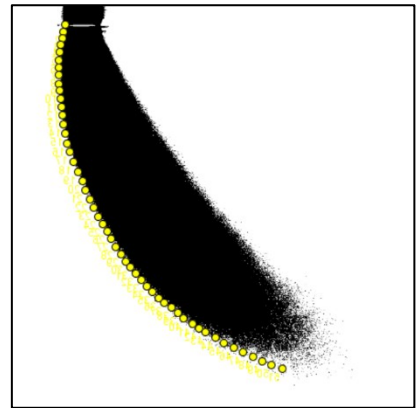
c) Averaged spray image



d) Averaged spray image after background subtraction



e) Thresholded image



f) Spray windward trajectory

Figure 3.6 Sample of shadowgraph images and image processing steps at  $GLR = 7\%$ ,  $q = 4$  and  $AR = 0.3$ .

### 3.2.4 Spray Droplet Size Analysis

One method to examine spray characterization is the analysis of droplet size data. In this study, the light diffraction method is used to measure the spray droplet size distribution in the gaseous crossflow. Figure 3.7 illustrates the setup for size measurement, including Spraytec (Malvern Panalytical, UK) and gas injection system in the test section.

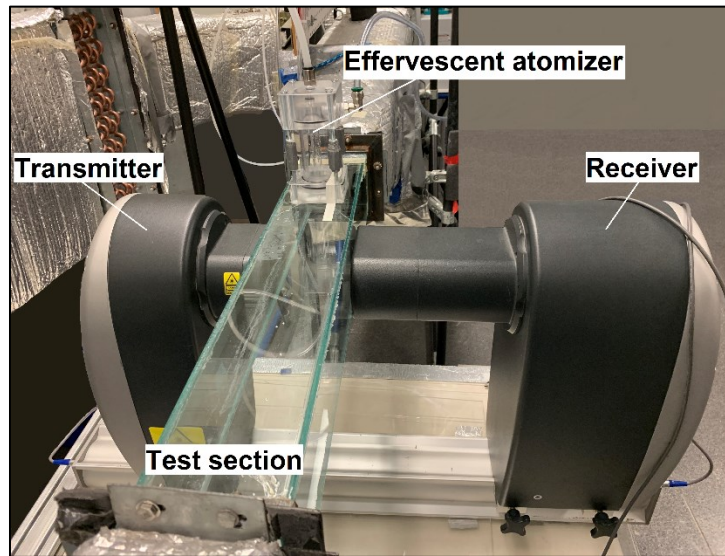


Figure 3.7 Malvern Spraytec setup.

The laser diffraction system uses a laser beam that passes through a spray where the intensity distribution of the scattered light is analyzed to measure the spray droplet sizes. It consists of a transmitter, a detector (receiver), an optical bench, which aligns the transmitter and detector, and Spraytec software to control the system and analyze data. The diameter of the laser beam is 10 mm. The test section is located between the transmitter and the receiver. All experiments are carried out along the test section centerline. Measurements are performed downstream at three x positions from the nozzle exit for four various heights from the top plane of the test section. Figure 3.8 shows the domain covered by measurement points to analyze droplet size distribution. Spray

droplet size is examined for  $q = 4$  at four gas to liquid mass ratios (GLR = 2, 4, 7 %) and three aspect ratios (AR = 3, 1, 0.3). The momentum flux ratio has little effect on the droplet size for the aerated circular jet in a crossflow [35].

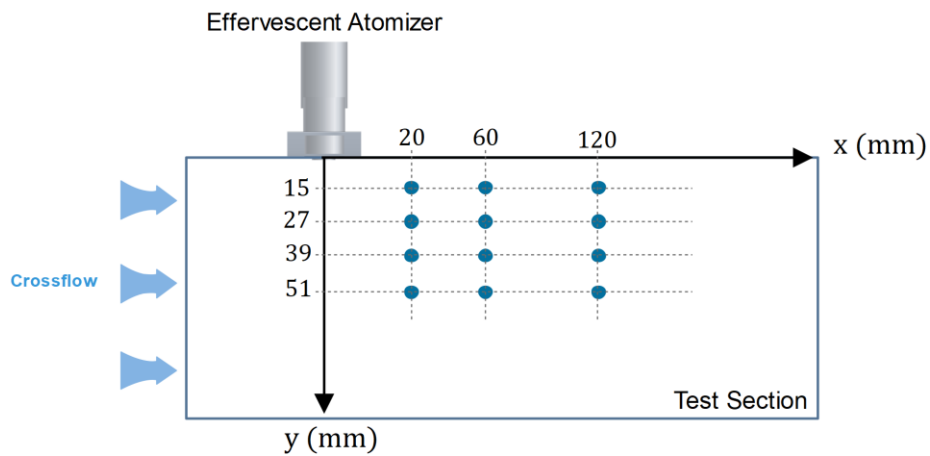


Figure 3.8 Measurement points for analyzing spray droplet size.

## 3.3 Results and Discussion

### 3.3.1 Near-Field

#### 3.3.1.1 Spray Visualization

In this section, the effervescent spray trajectory in a subsonic crossflow is visualized. Furthermore, the effects of orifice shape (elliptical and circular), air-liquid momentum flux ratio ( $q$ ) and gas-liquid mass flowrate ratio (GLR) on the jet trajectory and the penetration height are discussed.

Figure 3.9 shows nonaerated liquid jet ( $GLR = 0$ ) images in the gaseous crossflow for three different ARs. The effect of momentum flux ratio is evident in the shadowgraph images. As  $q$  increases, the spray penetration height for all aspect ratios increases too. Moreover,  $q$  has an effect on the jet disturbance growth. The jet surface is smooth at the highest  $q$  while it converts fully turbulent when  $q$  decreases. The turbulence effect on the elliptical jets is more apparent than that on the circular jet. One reason can be the existence of axis switching in elliptical jets. As Jadidi et al. [43] showed, the axis switching of elliptical jets causes a reduction in the breakup length. Hence, both axis switching and shorter breakup length make the elliptical jets more influenced by the turbulence effects of crossflow. At a fixed  $q$ , the penetration height of the circular jet is more than that of the elliptical jet. The spray from  $AR = 3$  seems to penetrate lower than the spray from  $AR = 0.3$ . A detailed plot is provided in the following section to compare the penetration height of  $AR = 0.3$  and  $AR = 3$ . This result shows that the orientation of an elliptical jet in a crossflow direction affects the spray trajectory. As Jadidi et al. [43] investigated, at a given  $q$ , the liquid jet of an elliptical orifice penetrates lower than the circular orifice. In other words, when  $AR < 1$ , the trajectory is slightly lower than  $AR = 1$  and much higher than  $AR > 1$ . In addition, Song et al. [56]

showed that the orifice aspect ratio affects the liquid jet trajectory in the air crossflow. They indicated that for elliptical nozzles with a similar equivalent diameter, the orifice with  $AR < 1$  has a higher liquid jet penetration than the orifice with  $AR > 1$ .

Figure 3.10-Figure 3.12 illustrate the spray images of aerated liquid jets ( $GLR \neq 0$ ) in a gaseous crossflow for GLRs of 2, 4 and 7%. It can be seen that elliptical and circular liquid jets penetrate higher when they get aerated compared to the nonaerated ones at the same  $q$ . In a thermal spray application, it is beneficial to reach high penetration without cooling the plasma significantly. The effervescent atomizer can achieve this purpose at a small liquid-gas momentum flux ratio ( $q = \rho_l U_l^2 / \rho_g U_g^2$ ) and low liquid flowrate by adding more gas to the nozzle. At a fixed  $q$ , the penetration height considerably increases by adding up to the amount of aerating gas, which has also been reported by Saleh et al. [38] for a circular atomizer. The reason is that when the liquid volume flowrate is kept constant, with an increase of atomizing gas, the thickness of the annular liquid sheath decreases. Therefore, the velocity of the annular liquid sheath and the effective momentum flux ratio increase. As a result of a rise in the effective momentum flux ratio, the penetration height increases. Lin et al. [34] also explained the influence of GLR on the spray penetration height. They stated to atomize a constant amount of liquid jet, the thickness of a liquid film reduces when the aeration level rises. Consequently, the liquid film velocity and the effective liquid-air momentum flux ratio increase with an aeration level. A series of plots are provided in the appendix section to show the impact of GLR on the spray penetration height. At a specific downstream location ( $x/d = 10$ ), when GLR increases from 0 to 7%, the spray penetration height ( $y/d$ ) has a growth of 18.8, 11.8 and 11.1 for  $AR = 1$ ,  $AR = 3$  and  $AR = 0.3$ , respectively. This rise in penetration heights means that the effect of being aerated is more noticeable on the penetration height of circular jets than that of elliptical jets.

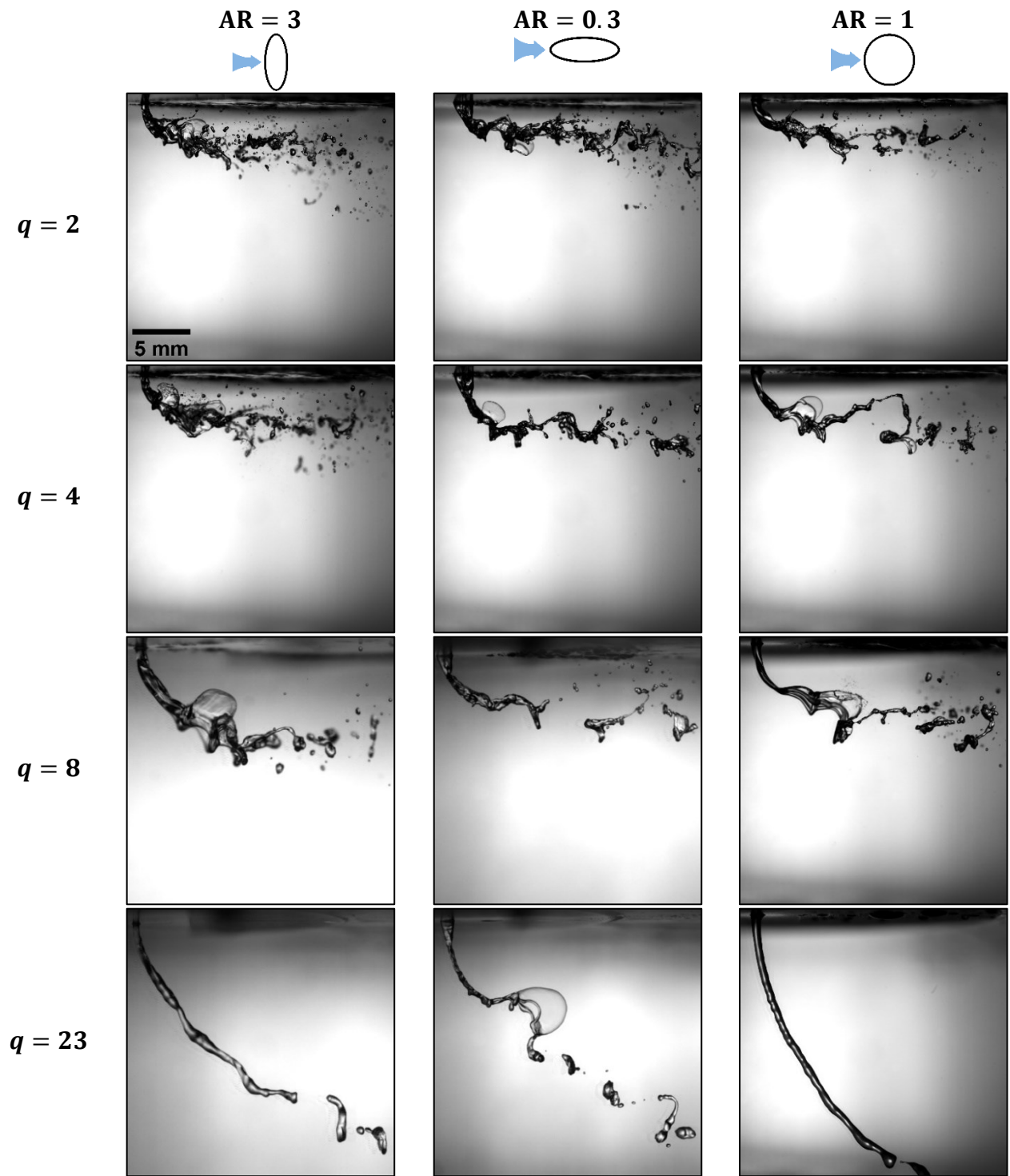


Figure 3.9 Shadowgraph images of non aerated liquid jet ( $GLR = 0$ ) in a gaseous crossflow.

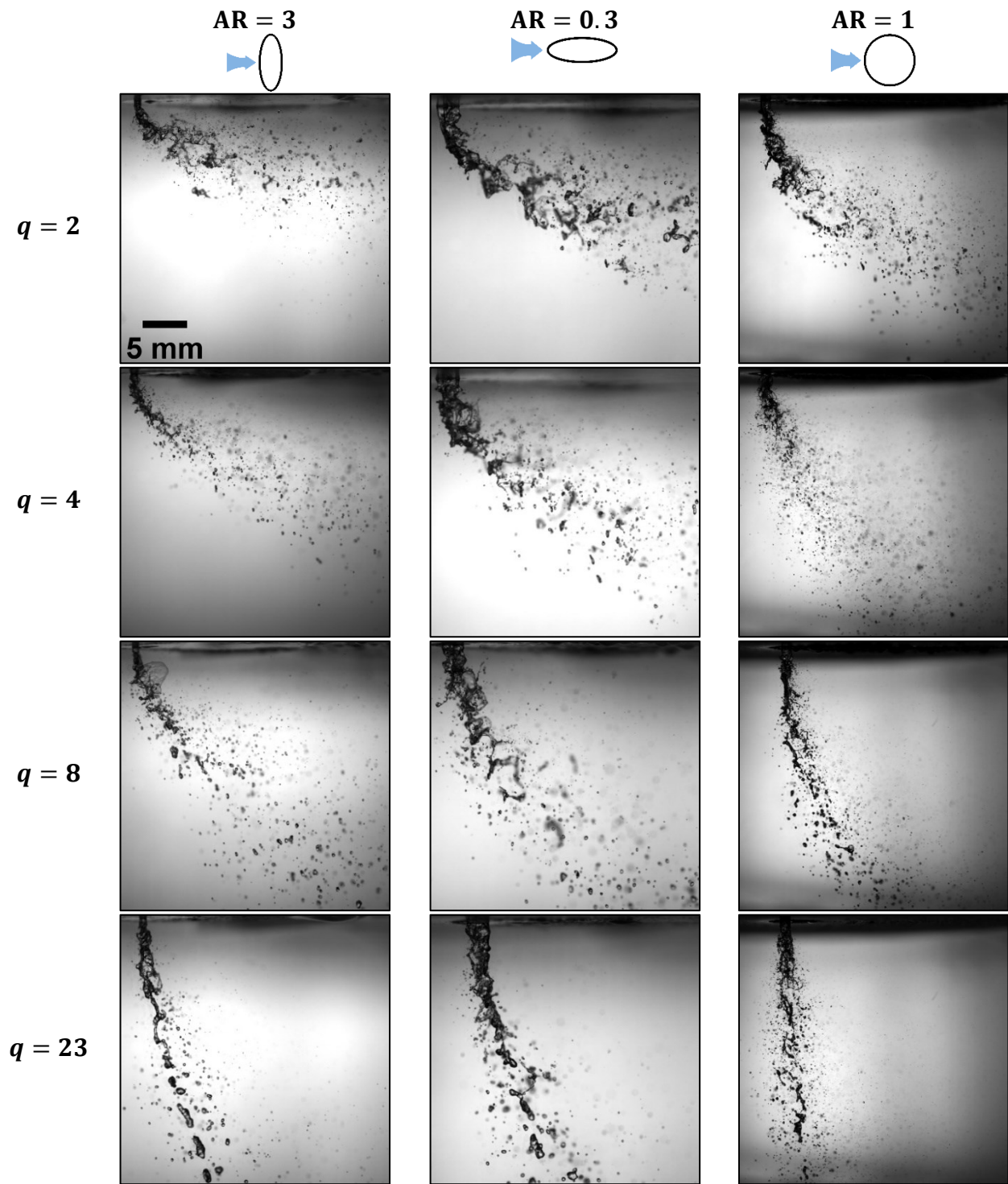


Figure 3.10 Shadowgraph images of the aerated spray (GLR = 2%) in a gaseous crossflow.

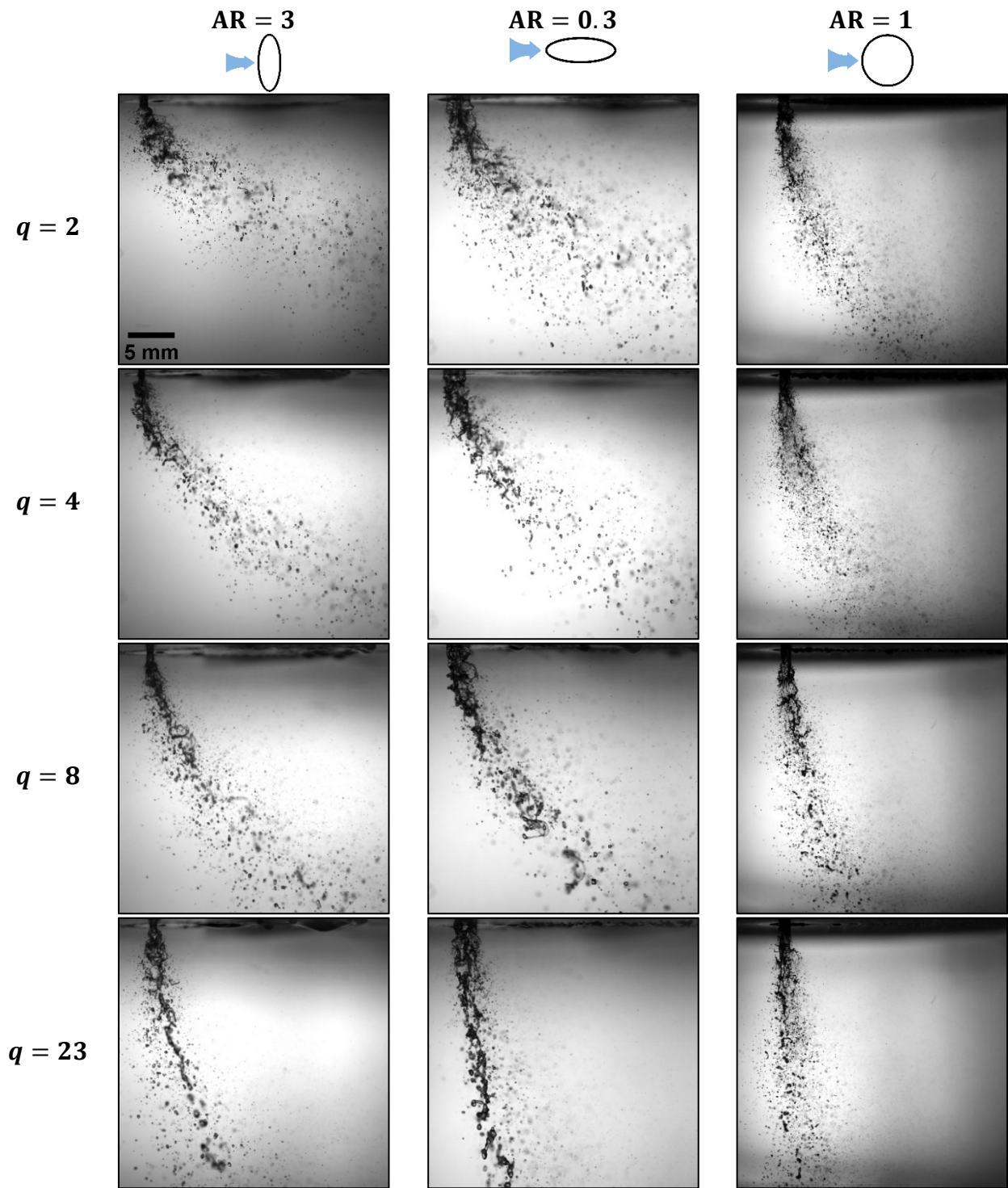


Figure 3.11 Shadowgraph images of the aerated spray (GLR = 4%) in a gaseous crossflow.

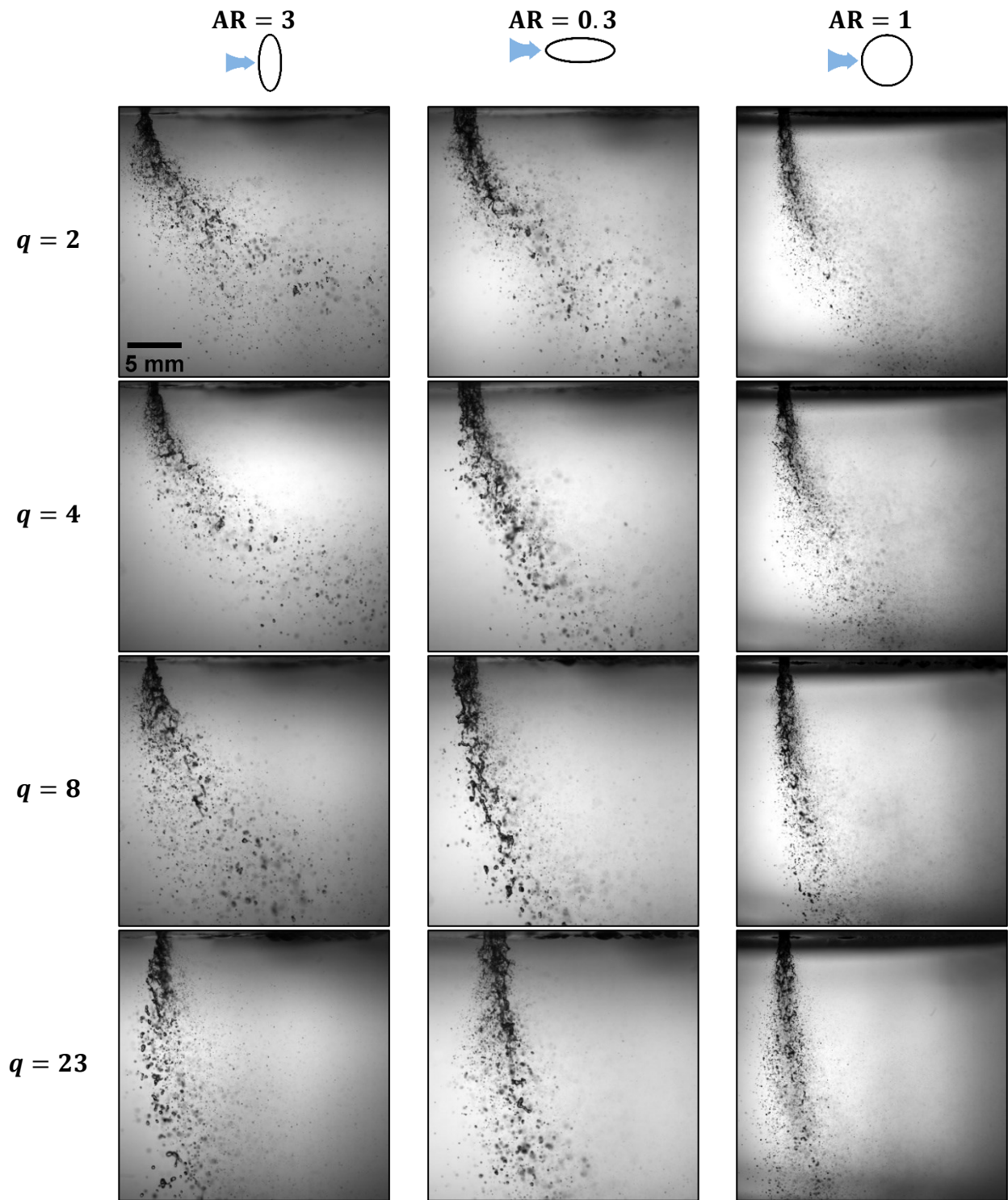


Figure 3.12 Shadowgraph images of the aerated spray (GLR = 7%) in a gaseous crossflow.

### 3.3.1.2 Penetration Height

Figure 3.13 shows the penetration heights versus downstream location, which are normalized by the orifice equivalent diameter and plotted for  $x/d < 30$  and  $y/d < 30$  for all experimental data.

In nonaerated jets ( $GLR = 0$ ) in crossflow, as discussed earlier, the circular liquid jet penetrates higher than the elliptical one. Furthermore, the jet penetration height of  $AR = 0.3$  is higher than that of  $AR = 3$ . Jadidi et al. [43] stated that the column breakup length of an elliptical jet is smaller than a circular one and droplets/ligaments are formed earlier in elliptical jets. Obviously, droplets and ligaments accelerate more than intact liquid columns in a crossflow direction. Therefore, it seems reasonable that elliptical jets have a lower penetration height than the equivalent circular jets. Furthermore, they indicated that the aspect ratio and presence of axis switching in elliptical jets influence the drag force, which is an essential factor in controlling the jet trajectory. When the major axis of an elliptical orifice is perpendicular to the crossflow ( $AR > 1$ ), the effect of drag force becomes more significant and results in less penetration.

For aerated liquid jets ( $GLR \neq 0$ ), the circular penetration height is deeper than the elliptical one. In effervescent atomizers, it has been shown that the liquid forms an annular sheath within the discharge orifice, which consequently breaks up into thin ligaments due to the expanding gas core [8], [19]. In an elliptical and circular discharge orifice with the same equivalent diameter, the thickness of an elliptical liquid film is thinner than its circular counterpart. Therefore, it disintegrates faster into droplets, which causes a shorter breakup length and lower penetration height. As a result, the aerated elliptical jet, regardless of its orientation, penetrates less into the crossflow than the aerated circular jet.

Another interesting phenomenon of the aerated liquid jets in crossflow is the backflow

formation on the windward side near the orifice exit. In the shadowgraph images and the penetration height plots provided here, it is seen that for  $AR = 3$ , the jet has a backflow immediately after the orifice discharge. However, for  $AR = 0.3$ , almost there is no backflow on the jet windward side when it goes out of the nozzle. It seems that the backflow formation influences the elliptical jet penetration height.

At  $q = 2$  for GLRs of 2, 4 and 7%, almost there is no backflow for the jet of  $AR = 3$ . Hence, its penetration height is less than  $AR = 0.3$  for each GLR, which is similar to the nonaerated cases ( $GLR = 0$ ). Because at  $q = 2$ , the crossflow velocity or the air momentum is high enough to overcome the jet momentum and does not allow the jet to have a backflow.

At  $q = 4$ , the crossflow momentum is not high enough to overcome the backflow of  $AR = 3$  when GLR increases. Hence, when GLR increases from 2 to 7%, the jet backflow of  $AR = 3$  increases, which causes a rise in its penetration height. In other words, at  $GLR = 2$ , the penetration height of  $AR = 3$  is considerably lower than  $AR = 0.3$ . However, as GLR increases, the penetration height of  $AR = 3$  rises and becomes almost similar to that of  $AR = 0.3$ .

At  $q = 8$ , the crossflow momentum is not enough to overcome the jet backflow. Hence, the backflow of  $AR = 3$  at  $q = 8$  is greater than that at  $q < 8$ . Moreover, increasing the GLR from 2 to 7% signifies the backflow, which causes a considerable growth in the penetration height of  $AR = 3$  compared to  $AR = 0.3$ .

For  $q = 23$ , the crossflow velocity is rather low where the jet cannot accelerate in the crossflow direction and the penetration of  $AR = 3$  and  $AR = 0.3$  is almost identical. Consequently, the existence of backflow in an aerated elliptical jet causes a rise in the penetration height. As it is evident, the spray instabilities, the thresholding uncertainties of image processing and instrument error are the sources of uncertainty in the calculated penetration heights.

Some plots are provided to display the effect of GLR and  $q$  on the spray penetration height, which are shown in the appendices. For all conditions, the penetration height increases when  $q$  or GLR increases. For elliptical and circular jets, when  $q$  is high, the impact of aeration level (GLR) on the jet trajectory is slightly noticeable. However, at a low  $q$ , the aeration level effect on the jet trajectory is highly apparent.

In aerated circular jets, the penetration height is influenced by GLR more than in the aerated elliptical jets. Hence, the aeration level can increase the effective momentum of circular liquid jets to penetrate higher in a gaseous crossflow. Therefore, the crossflow velocity rise influences the aerated circular jet trajectory less than the aerated elliptical jet trajectory. The following empirical correlation calculated for all experimental data can prove the effect of GLR and  $q$  on circular and elliptical jets.

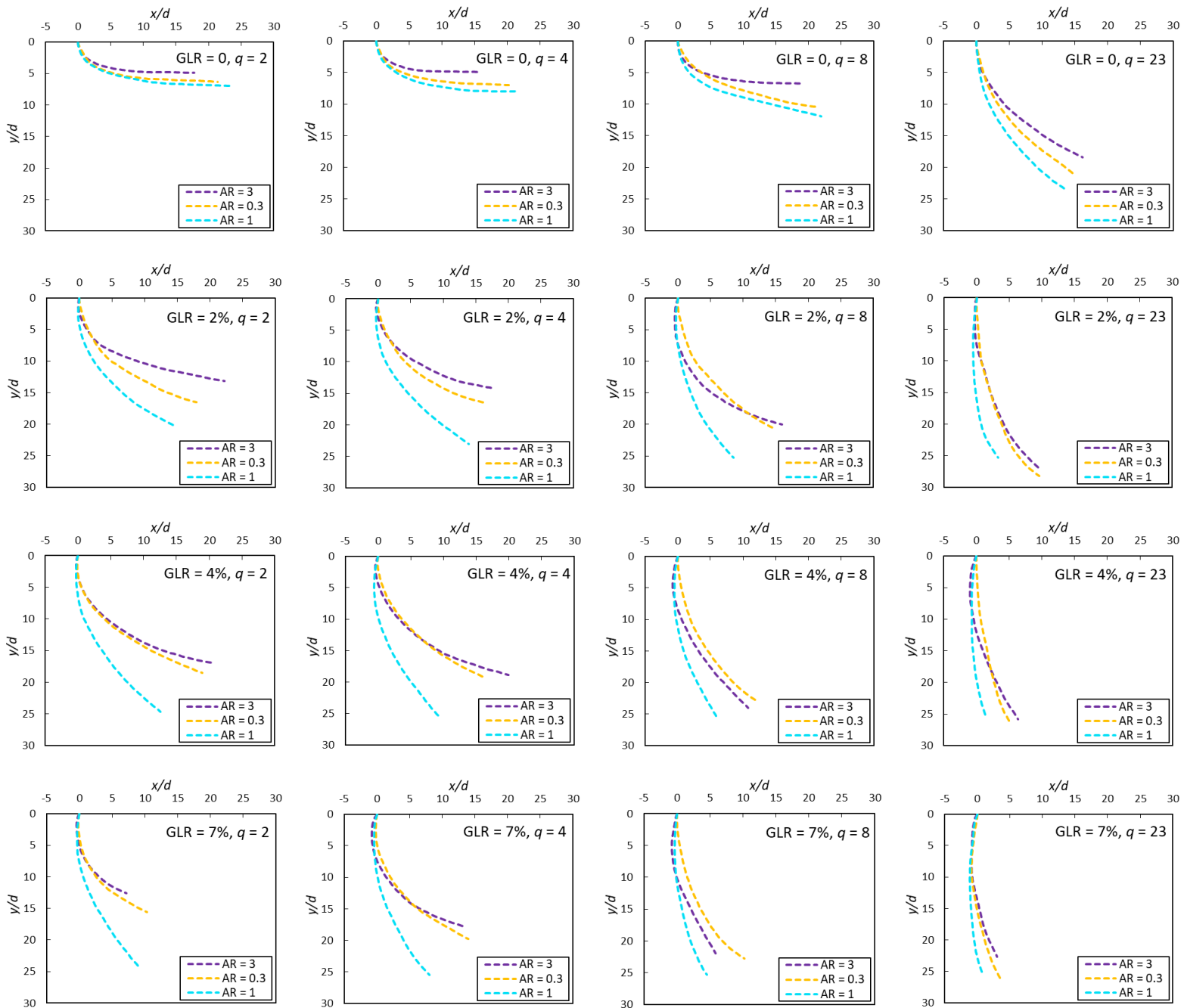


Figure 3.13 Effect of aspect ratio on the spray trajectory at various  $q$  and GLR.

An empirical correlation, which estimates the spray penetration height, is obtained based on data points collected from the jet trajectories of all test conditions. This correlation is a function of the momentum flux ratio ( $q$ ), the normalized downstream location ( $x / d$ ), the gas-liquid mass ratio (GLR) and the aspect ratio (AR). The jet trajectory correlation, which is valid for  $x / d > 1$ , is given by Eq. 1:

$$\frac{y}{d} = 5.75 q^{0.42} \left(\frac{x}{d}\right)^{0.37} \frac{(0.46 + \text{GLR})^{0.42}}{\left(\text{AR} + \frac{1}{\text{AR}}\right)^{0.86}} \quad \text{Eq. 1}$$

where  $R^2$ , the goodness of fit, is 0.94 and the mean squared error is 2.59. This equation format has been selected based on the most commonly used correlation formats for the jet in crossflow to be comparable to other existing equations [38], [43], [51].

As Eq. 1 shows, the momentum flux ratio strongly affects the spray penetration height. By increasing the amount of  $q$ , spray penetrates higher in a gaseous crossflow. The effect of aspect ratio, which is plotted in Figure 3.13, is predicted by Eq. 1. The penetration height of the circular orifice ( $\text{AR} = 1$ ) is more than the elliptical orifice. Moreover, the penetration heights of  $\text{AR} = 0.3$  and  $\text{AR} = 3$  are almost equal. The penetration height predicted by Eq. 1 is compared with the obtained data from experimental measurements in Figure 3.14.

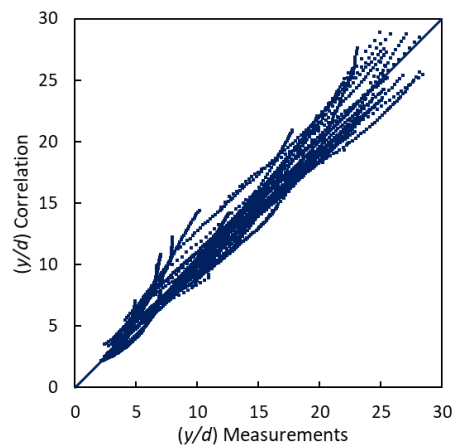


Figure 3.14 Comparison of experimental data and predicted values by Eq. 1.

## 3.3.2 Far-field

### 3.3.2.1 Droplet Size Distribution

The droplet size of the aerated liquid jet in crossflow is measured by the laser diffraction technique. In Figure 3.15- Figure 3.17, the distribution of Sauter Mean Diameter ( $D_{32}$ ) is plotted versus  $x$  and  $y$  position. The measurement points are shown by red dots. The spray shadowgraph images are scaled and placed on these plots to demonstrate the far field measurement domain better. In all experiments, the standard deviation of SMD for each measurement point is less than 15%. At a fixed downstream location, as the height ( $y$ ) increases the SMD increases for all ARs and all GLRs. Hence, larger droplets are mainly around the windward area. Moreover, at a specific height, droplets become smaller as they move in the downstream direction, mainly due to secondary breakup and droplet evaporation. As seen in Figure 3.15, at the largest GLR value (7%), both elliptical and circular sprays are fully atomized and most of the measurement domain is blue, which demonstrates that particle sizes are mainly small. At lower GLRs (2 – 4%), there is an area without data in the SMD plots of AR = 3 and AR = 0.3. The reason is that the number of droplets is low at these measurement points due to the low penetration height. As discussed earlier, the penetration height of a circular jet is higher than an elliptical jet, therefore there is no blank area in the plots of AR = 1. It is seen that the SMD of circular and elliptical jets at each measurement point becomes more identical when GLR increases. At low GLRs, the SMD of the circular jet is smaller than that of the elliptical jet. However, the SMD of AR = 3 and AR = 0.3 are almost identical at each measurement point for all GLRs.

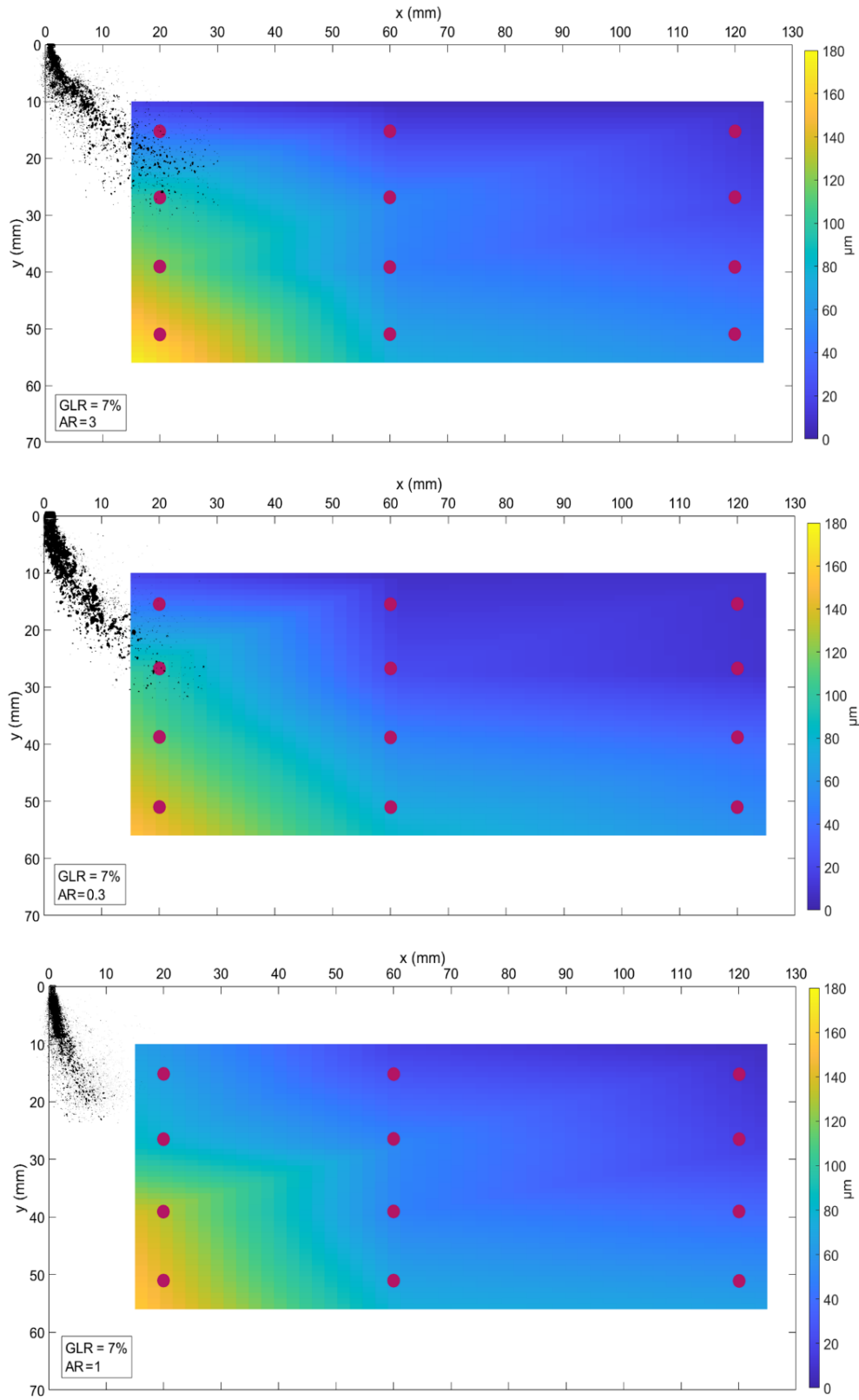


Figure 3.15 Droplet size contour for different aspect ratios at  $\text{GLR} = 7\%$  and  $q = 4$ , the color map shows SMD (0 – 180  $\mu\text{m}$ ).

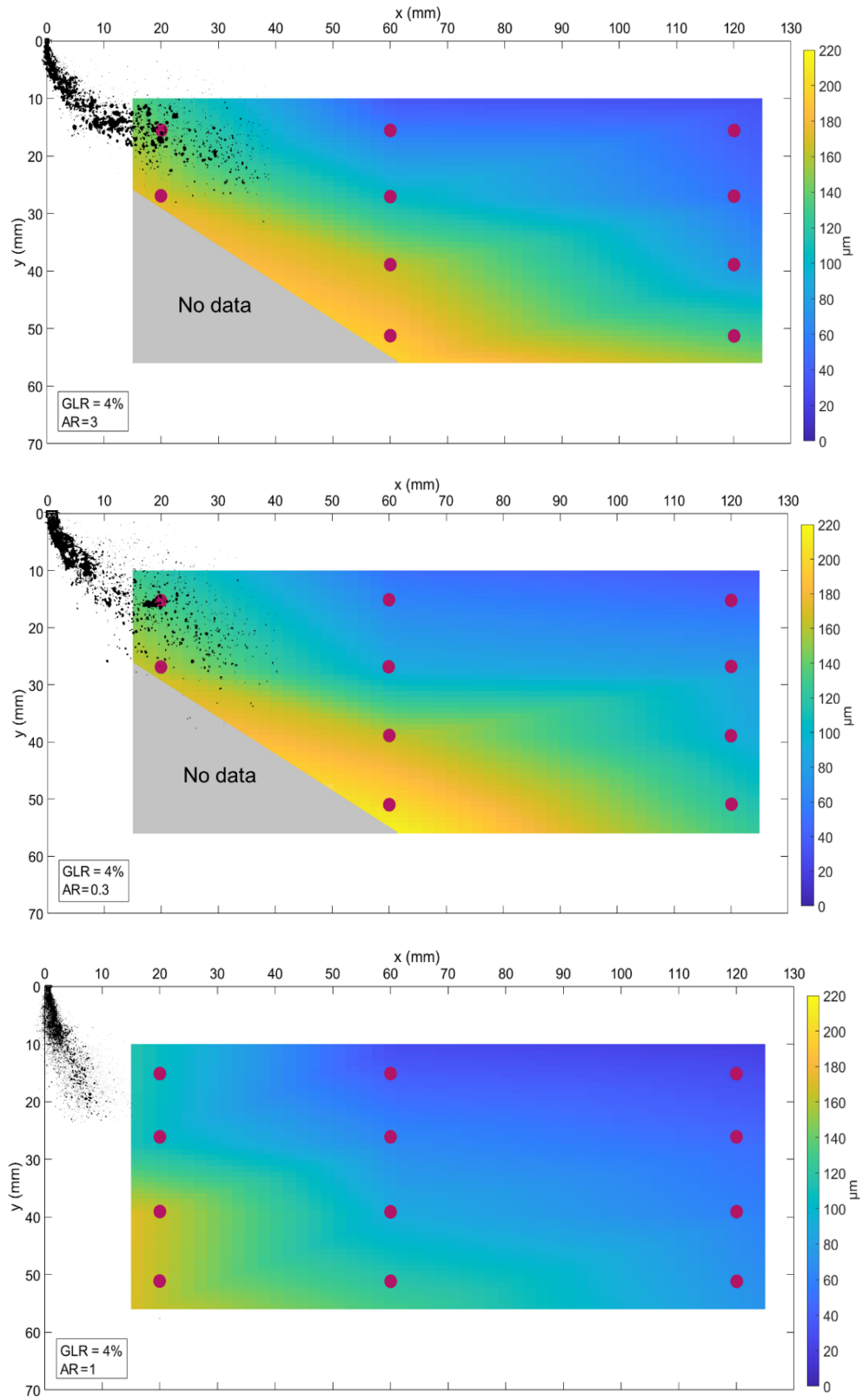


Figure 3.16 Droplet size contour for different aspect ratios at  $\text{GLR} = 4\%$  and  $q = 4$ , the color map shows SMD (0 – 220  $\mu\text{m}$ ).

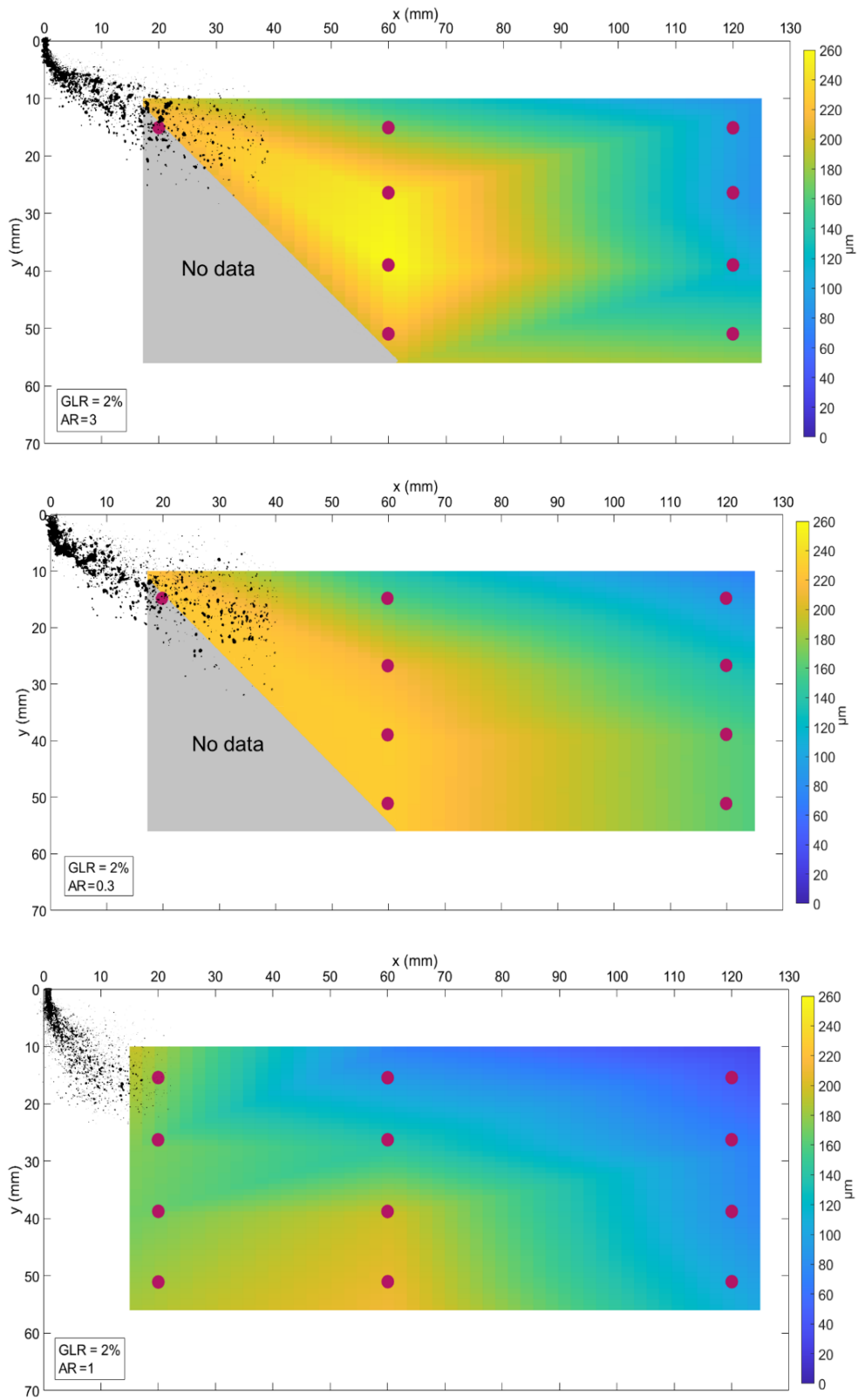


Figure 3.17 Droplet size contour for different aspect ratios at  $\text{GLR} = 2\%$  and  $q = 4$ , the color map shows SMD (0 – 260  $\mu\text{m}$ ).

To show the effect of aspect ratio (AR) and gas-liquid mass flow rate ratio (GLR) on the spray droplet size, the weighted ensemble averaging along the  $y$ -direction is applied on the SMD data at each  $x$  position. The volume concentration expressed in PPM (parts per million) is considered as the weight for SMD data in this averaging method. Hence, particle sizes with a higher volume concentration have a higher weight in the resultant averaged SMD. Figure 3.18 and Figure 3.19 show the weighted average of SMD at each downstream location for  $AR = 0.3, 1, 3$  and  $GLR = 2 - 7\%$ .

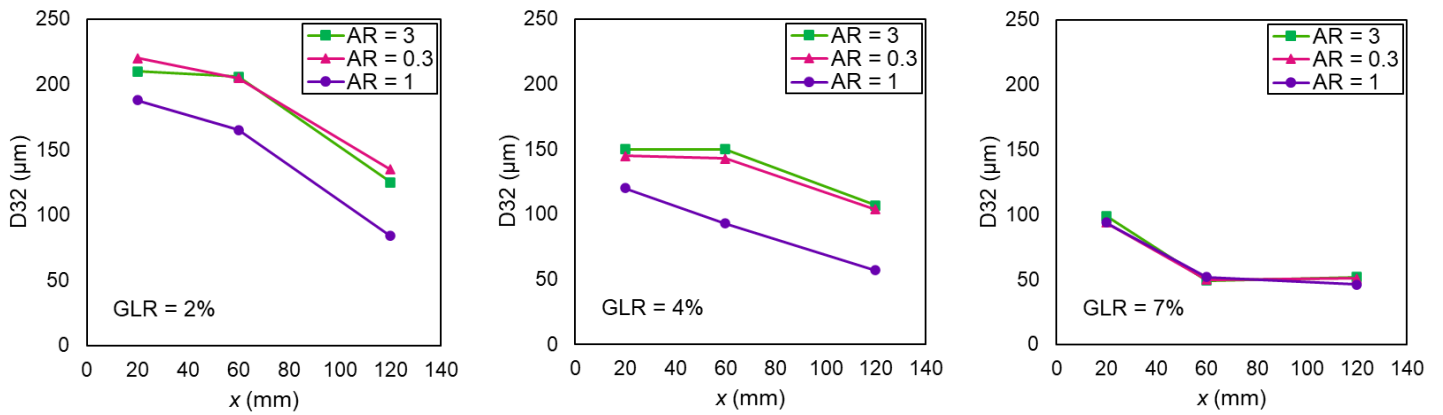


Figure 3.18 Weighted ensemble average of SMD versus downstream location for various GLRs and aspect ratios at  $q = 4$ .

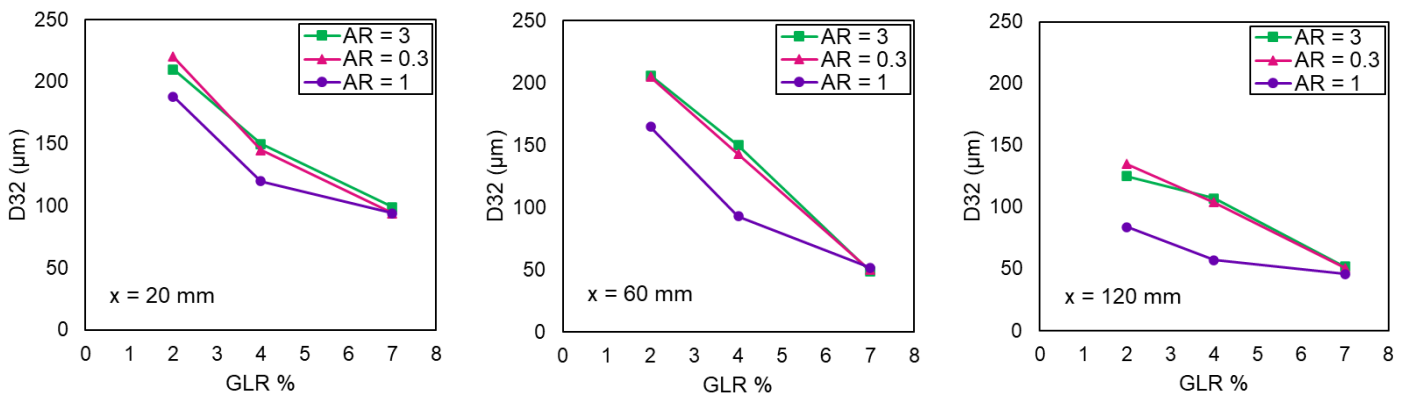


Figure 3.19 Weighted ensemble average of SMD versus GLR at three downstream locations for various aspect ratios at  $q = 4$ .

Figure 3.18 illustrates the effect of downstream location ( $x$ ) on the SMD of elliptical and circular jets at various GLRs. At each GLR, with increasing of  $x$ , the SMD generally reduces. The reason for smaller droplet sizes in downstream distances can be the secondary breakup, which has been reported in the literature for aerated circular jets in crossflow. As  $x$  rises, it is seen that the secondary breakup causes a reduction in the SMD of the aerated elliptical jet as well as the aerated circular jet. Miller et al. [35] and Lee et al. [36] showed that in an aerated circular jet, the secondary breakup reduces droplet sizes as they move downstream.

At low GLR (2%), the secondary breakup affects the SMD mainly after the downstream distance of 60 mm. Hence, for both elliptical and circular jets, the SMD noticeably reduces after  $x = 60$  mm. At GLR = 4%, it seems that the secondary breakup effect on the elliptical jet is different from that on the circular jet. As it is seen, there is a constant reduction in the SMD of AR = 1 between  $x = 20 - 60$  mm and  $x = 60 - 120$  mm. However, for AR = 0.3 and AR = 3, the secondary breakup effect on the SMD is more evident after  $x = 60$  mm. The SMD is almost constant between  $x = 20 - 60$  mm while it considerably decreases after the distance of 60 mm. At GLR = 7%, the secondary breakup affects the SMD mainly before  $x = 60$  mm. Hence, there is a considerable reduction in the SMD of all aspect ratios between  $x = 20 - 60$  mm. For downstream locations farther than 60 mm, the SMD generally remains constant.

Figure 3.18 shows that the SMD of AR = 3 and AR = 0.3 are generally identical at each downstream location for each GLR. Moreover, the aerated circular jet generates smaller droplet sizes than the aerated elliptical jet at GLRs lower than 7%. However, at GLR = 7%, the SMD of both elliptical and circular jets is similar at each  $x$  location. Consequently, higher aeration levels can diminish the orifice shape effect on the spray droplet size in gaseous crossflow, which is demonstrated better in Figure 3.19. At each  $x$  location, when GLR increases from 2 to 7%, the SMD

decreases in the elliptical jet as well as the circular jet. Miller et al. [35] indicated that GLR has the most effect on the droplet size of an aerated circular jet in subsonic crossflow. They stated that as GLR rises, the liquid film squeezes into a thinner sheet because of the increased gas flow rate, which causes a reduction in the SMD. Here, it is seen that the effect of GLR on the SMD of the elliptical jet is more than that of a circular jet. In other words, at each  $x$  location, the SMD of  $AR = 3$  and  $AR = 0.3$  has a broader variation span compared to  $AR = 1$  when the aeration level rises from  $GLR = 2$  to  $7\%$ .

### 3.4 Conclusion

Effervescent atomization in a subsonic crossflow has been analyzed experimentally in the current study. The effect of orifice shape on the spray atomization in crossflow, including jet penetration height and droplet size, has been studied. Aspect ratios of 0.3, 1, and 3 have been analyzed at different gas-liquid mass flowrate ratios ( $GLR = 0 - 7\%$ ) and various momentum flux ratios ( $q = 2 - 23$ ). The high-speed shadowgraphy and the laser diffraction techniques have been used to study the jet trajectory and droplet size, respectively.

It is concluded that increasing the aeration level ( $GLR$ ), as well as increasing the momentum flux ratio ( $q$ ), results in higher penetration into the crossflow for all aspect ratios. The results show that the circular jet has a higher penetration height than the elliptical jet at all  $GLRs$  and all  $qs$ . Moreover, the backflow formation influences the elliptical jet penetration height when the major diameter is perpendicular to the crossflow ( $AR = 3$ ). Generally, the combined effects of backflow,  $GLR$  and  $q$  cause  $AR = 0.3$  to penetrate higher than  $AR = 3$  at most conditions and penetrate less at the remaining conditions.

To compare the droplet size of the aerated elliptical jet with that of the aerated circular jet, the weighted average of Sauter Mean Diameter ( $SMD$ ) has been calculated at each measurement point for  $GLR = 2, 4, 7\%$  and for  $q = 4$ . The obtained  $SMDs$  reveal that as the aeration level increases, both elliptical and circular orifices generate smaller droplets. At  $GLR < 7\%$ , the circular spray has a smaller  $SMD$  than the elliptical spray, while at  $GLR = 7\%$ , the  $SMDs$  of circular and elliptical jets are generally identical at each downstream location. Moreover, as droplets travel downstream locations, they become smaller as a result of the secondary breakup and evaporation. In the aerated elliptical jet in crossflow, the droplet size is independent of the orifice orientation

with respect to the crossflow direction. In other words, the SMD of both aspect ratios of the elliptical jet ( $AR = 3$  and  $AR = 0.3$ ) is mostly identical at each GLR and each downstream location.

## 4 Summary, Conclusions and Recommendations for Future Work

### 4.1 Summary and Conclusions

This study is divided into two separate parts. In the first part, effervescent atomization in the quiescent air condition is experimentally studied and in the second part, the behavior of effervescent atomization in a gaseous crossflow is examined. First, the spray angle of an effervescent atomizer with an elliptical orifice is measured from the minor axis and major axis views. The gas-liquid mass flowrate ratios are from 0.5 to 2.5%, where the gas flow rate varies between 1780 – 8423 mL/min. The high-speed imaging method is employed to capture the spray frames from two views of the elliptical orifice. For each test condition, the average image, which is the superimposition of 800 frames, is used to measure the average spray angle. The results show that the spray has a wider angle from the minor view than the major view. Since the smaller diameter of the minor axis side increases the strength of bubble bursting, which splashes water in a broader domain. This phenomenon causes the presence of the backflow on the windward side. Additionally, the aerating gas energy depends on the amount of air existing for the atomization of water. The spray angle increases by increasing the aeration level; for example, the spray angle at the GLR of 0.5% is approximately 8 degrees, which goes up to 20 degrees at the higher GLR of 2.55%.

In the second part, effervescent atomization in a subsonic crossflow is studied experimentally. The effect of orifice shape on the atomization characteristics, such as spray trajectory in a crossflow and drop size distribution, is investigated. Three aspect ratios ( $AR = 0.3, 1, 3$ ) are examined at various gas-liquid mass flowrate ratios ( $GLR = 0 - 7\%$ ) and different liquid-air momentum flux ratios ( $q = 2 - 23$ ). The high-speed shadowgraph technique is used to

calculate the spray penetration in a gaseous crossflow. Besides, the laser diffraction technique is employed to find the droplet size distributions.

It is found that the spray penetration height of all aspect ratios increases with a rise in GLR or  $q$ . The results show that the circular jet penetrates a crossflow higher than the elliptical jet for all GLR and  $q$  values. The elliptical jet penetration height is influenced by the backflow formation when the major diameter is perpendicular to the crossflow direction ( $AR = 3$ ). Hence, the combined effects of GLR,  $q$  and backflow highly affect the jet trajectory of  $AR = 3$ . Generally, at most test conditions, the aerated jet of  $AR = 3$  penetrates less than  $AR = 0.3$ . The backflow formation can be explained by examining the spray angles calculated in the first part. The smaller diameter of the minor axis side increases the gas core energy to shatter the liquid film at a wider angle resulting in a backflow near the spray discharge when the minor diameter is in the same direction of the crossflow.

The weighted average of Sauter Mean Diameter (SMD) is calculated for the aerated circular and elliptical jets in a gaseous crossflow for  $GLR = 2, 4, 7\%$  and  $q = 4$ . The results show that the SMD decreases in both circular and elliptical sprays as GLR increases. When  $GLR < 7\%$ , the droplets of circular spray are smaller than the elliptical spray, while at  $GLR = 7\%$ , the droplet sizes of circular and elliptical sprays are mostly similar at each downstream location. Moreover, as droplets move downstream, the SMD reduces in the aerated circular and elliptical sprays because of the secondary breakup and droplet evaporation. It is found that the droplet size of the aerated elliptical jet is independent of the orifice orientation in a crossflow. Consequently, the SMD is almost identical for  $AR = 3$  and  $AR = 0.3$  at each GLR and each downstream location.

## 4.2 Future Work

In the present study, penetration height and droplet size distribution of effervescent atomization in a subsonic crossflow with elliptical and circular orifices have been investigated. Besides, the effects of aeration level of atomization and liquid-air momentum flux ratio have been analyzed. However, the effect of a broader range of ellipticity on twin-fluid atomization in a crossflow is not fully recognized. Hence, more experimental and numerical studies are needed to find the best aspects of elliptical orifices for aerated atomization in crossflow applications. There are some recommendations for future research related to effervescent atomizers with an elliptical discharge orifice:

- For effervescent atomization in gaseous crossflow, the effect of orifice ellipticity can be investigated by examining a wider range of aspect ratios.
- Higher GLRs (more than 7%) may affect the droplet size distribution pattern of elliptical jets.
- As many parameters affecting the spray trajectory in a gaseous crossflow, the experimental data is large. Consequently, using machine learning to predict the spray trajectory and generate the empirical correlation can be very helpful.
- Applying Proper Orthogonal Decomposition (POD), Spectral Proper Orthogonal Decomposition (SPOD) and Dynamic Mode Decomposition (DMD) analyses on the experimental data of an aerated liquid jet in crossflow can be incredibly beneficial to find the dynamic flow structure.
- Numerically simulate an effervescent atomizer with an elliptical orifice in a crossflow enables researchers to examine more comprehensive test conditions that are limited physically to experiment.

## Reference

- [1] W. Bachalo, "Spray Diagnostics for the Twenty-First Century," *Atomization and Sprays*, vol. 10, pp. 439–474, May 2000, doi: 10.1615/AtomizSpr.v10.i3-5.110.
- [2] A. H. Lefebvre and V. G. McDonell, *Atomization and Sprays*. CRC Press, 2017.
- [3] E. Michaelides, C. T. Crowe, and J. D. Schwarzkopf, *Multiphase Flow Handbook, Second Edition*. CRC Press, 2016.
- [4] A. H. Lefebvre, X. F. Wang, and C. A. Martin, "Spray characteristics of aerated-liquid pressure atomizers," *Journal of Propulsion and Power*, vol. 4, no. 4, pp. 293–298, Jul. 1988, doi: 10.2514/3.23066.
- [5] A. H. Lefebvre, "A novel method of atomization with potential gas turbine applications," *Defense Science Journal*, vol. 38, pp. 353–361, Oct. 1988.
- [6] T. C. Roesler and A. H. Lefebvre, "Studies on Aerated-Liquid Atomization," *International Journal of Turbo & Jet-Engines*, vol. 6, no. 3–4, pp. 221–230, Dec. 1989, doi: 10.1515/TJJ.1989.6.3-4.221.
- [7] X. F. Wang, J. S. Chin, and A. H. Lefebvre, "Influence of Gas-Injector Geometry on Atomization Performance of Aerated-Liquid Nozzles," *International Journal of Turbo & Jet-Engines*, vol. 6, no. 3–4, pp. 271–280, Dec. 1989, doi: 10.1515/TJJ.1989.6.3-4.271.
- [8] S. D. Sovani, P. E. Sojka, and A. H. Lefebvre, "Effervescent atomization," *Progress in Energy and Combustion Science*, vol. 27, no. 4, pp. 483–521, Jan. 2001, doi: 10.1016/S0360-1285(00)00029-0.
- [9] Buckner, Harry N., and Paul E. Sojka, "Effervescent Atomization of High-Viscosity Fluids: Part I. Newtonian Liquids," *Atomization and Sprays*, Volume 1, 1991, Issue 3 - Begell House Digital Library.
- [10] M. T. Lund, P. E. Sojka, A. H. Lefebvre, and P. G. Gosselin, "Effervescent Atomization at Low Mass Flow Rates. PART I: The Influence of Surface Tension," *AAS*, vol. 3, no. 1, 1993, doi: 10.1615/AtomizSpr.v3.i1.40.
- [11] J. J. Sutherland, P. E. Sojka, and M. W. Plesniak, "Ligament-Controlled Effervescent Atomization," *AAS*, vol. 7, no. 4, 1997, doi: 10.1615/AtomizSpr.v7.i4.40.
- [12] M. V. Panchagnula and P. E. Sojka, "Spatial droplet velocity and size profiles in effervescent atomizer-produced sprays," *Fuel*, vol. 78, no. 6, pp. 729–741, May 1999, doi: 10.1016/S0016-2361(98)00192-6.

- [13] M. R. Satapathy, S. Sovani, P. E. Sojka, J. Gore, W. A. Eckerle, and J. D. Crofts, "The effect of ambient density on the performance of an effervescent atomizer operating in the MPa injection pressure range," *Proceedings of the Technical Meeting of the Central States Section of the Combustion Institute*, pp. 76–80, Jan. 1998.
- [14] J. D. Whitlow, A. H. Lefebvre, and R. J. Rollbuhler, "Experimental studies on effervescent atomizers with wide spray angles," Sep. 1993.
- [15] S. K. Chen, A. H. Lefebvre, and J. Rollbuhler, "Influence of ambient air pressure on effervescent atomization," *Journal of Propulsion and Power*, vol. 9, no. 1, pp. 10–15, Jan. 1993, doi: 10.2514/3.11479.
- [16] S. K. Chen and A. H. Lefebvre, "Spray cone angles of effervescent atomizers," *AAS*, vol. 4, no. 3, 1994, doi: 10.1615/AtomizSpr.v4.i3.40.
- [17] S. G. Bush, J. B. Bennett, P. E. Sojka, M. V. Panchagnula, and M. W. Plesniak, "Momentum rate probe for use with two-phase flows," *Review of Scientific Instruments*, vol. 67, no. 5, pp. 1878–1885, May 1996, doi: 10.1063/1.1146992.
- [18] F. J. Petersen, O. Wørts, T. Schæfer, and P. E. Sojka, "Design and Atomization Properties for an Inside-Out Type Effervescent Atomizer," *Drug Development and Industrial Pharmacy*, vol. 30, no. 3, pp. 319–326, Jan. 2004, doi: 10.1081/DDC-120030427.
- [19] P. J. Santangelo and P. E. Sojka, "A Holographic Investigation of the Near-Nozzle Structure of an Effervescent Atomizer-Produced Spray," *AAS*, vol. 5, no. 2, 1995, doi: 10.1615/AtomizSpr.v5.i2.20.
- [20] J. Jedelsky, J. Otáhal, and M. Jicha, "Effervescent atomizer: influence of the internal geometry on atomization performance," 2007.
- [21] A. Mostafa, M. Fouad, M. Enayet, and S. Osman, "Measurements of Spray Characteristics Produced by Effervescent Atomizers," in *40th AIAA/ASME/SAE/ASEE Joint Propulsion Conference and Exhibit*, American Institute of Aeronautics and Astronautics.
- [22] J. S. Chin and A. H. Lefebvre, "A Design Procedure for Effervescent Atomizers," *ASME. J. Eng. Gas Turbines Power*. April 1995; 117(2): 266–271.
- [23] K. W. Ku, J. G. Hong, and C.-W. Lee, "Effect of Internal Flow Structure in Circular and Elliptical Nozzles on Spray Characteristics," *AAS*, vol. 21, no. 8, 2011, doi: 10.1615/AtomizSpr.2012004192.
- [24] T. V. Kasyap, D. Sivakumar, and B. N. Raghunandan, "Breakup of Liquid Jets Emanating From Elliptical Orifices at Low Flow Conditions," *AAS*, vol. 18, no. 7, 2008, doi: 10.1615/AtomizSpr.v18.i7.30.
- [25] T. V. Kasyap, D. Sivakumar, and B. N. Raghunandan, "Flow and breakup characteristics of

elliptical liquid jets,” *International Journal of Multiphase Flow*, vol. 35, no. 1, pp. 8–19, Jan. 2009, doi: 10.1016/j.ijmultiphaseflow.2008.09.002.

- [26] M. Marzbali, “Penetration of circular and elliptical liquid jets into gaseous crossflow: a combined theoretical and numerical study,” PhD Thesis, Concordia University, 2011.
- [27] P.-K. Wu, K. A. Kirkendall, R. P. Fuller, and A. S. Nejad, “Spray Structures of Liquid Jets Atomized in Subsonic Crossflows,” *Journal of Propulsion and Power*, vol. 14, no. 2, pp. 173–182, Mar. 1998, doi: 10.2514/2.5283.
- [28] J. N. Stenzler, J. G. Lee, D. A. Santavicca, and W. Lee, “Penetration of Liquid Jets in a Cross-Flow,” *AAS*, vol. 16, no. 8, 2006, doi: 10.1615/AtomizSpr.v16.i8.30.
- [29] D. Sedarsky *et al.*, “Model validation image data for breakup of a liquid jet in crossflow: part I,” *Experiments in fluids*, vol. 49, no. 2, pp. 391–408, 2010.
- [30] E. Farvardin, M. Johnson, H. Alaei, A. Martinez, and A. Dolatabadi, “Comparative Study of Biodiesel and Diesel Jets in Gaseous Crossflow,” *Journal of Propulsion and Power*, vol. 29, no. 6, pp. 1292–1302, 2013, doi: 10.2514/1.B34743.
- [31] M. Behzad, N. Ashgriz, and A. Mashayek, “Azimuthal shear instability of a liquid jet injected into a gaseous cross-flow,” *Journal of Fluid Mechanics*, vol. 767, pp. 146–172, Mar. 2015, doi: <http://dx.doi.org/10.1017/jfm.2015.36>.
- [32] M. Jadidi, S. Moghtadernejad, and A. Dolatabadi, “Penetration and breakup of liquid jet in transverse free air jet with application in suspension-solution thermal sprays,” *Materials & Design*, vol. 110, pp. 425–435, Nov. 2016, doi: 10.1016/j.matdes.2016.07.145.
- [33] A. Amighi and N. Ashgriz, “Global Droplet Size in Liquid Jet in a High-Temperature and High-Pressure Crossflow,” *AIAA Journal*, vol. 57, no. 3, pp. 1260–1274, 2019, doi: 10.2514/1.J056496.
- [34] K.-C. Lin, P. Kennedy, and T. Jackson, “Structures of aerated-liquid jets in subsonic crossflows,” in *39th Aerospace Sciences Meeting and Exhibit*, American Institute of Aeronautics and Astronautics.
- [35] B. Miller, K. A. Sallam, M. Bingabr, K.-C. Lin, and C. Carter, “Breakup of Aerated Liquid Jets in Subsonic Crossflow,” *Journal of Propulsion and Power*, vol. 24, no. 2, pp. 253–258, Mar. 2008, doi: 10.2514/1.30390.
- [36] J. Lee, K. A. Sallam, K.-C. Lin, and C. D. Carter, “Spray Structure in Near-Injector Region of Aerated Jet in Subsonic Crossflow,” *Journal of Propulsion and Power*, vol. 25, no. 2, pp. 258–266, Mar. 2009, doi: 10.2514/1.36719.
- [37] D. S. Olinger, K. A. Sallam, K.-C. Lin, and C. D. Carter, “Digital Holographic Analysis of the Near Field of Aerated-Liquid Jets in Crossflow,” *Journal of Propulsion and Power*, vol.

30, no. 6, pp. 1636–1645, 2014, doi: 10.2514/1.B34984.

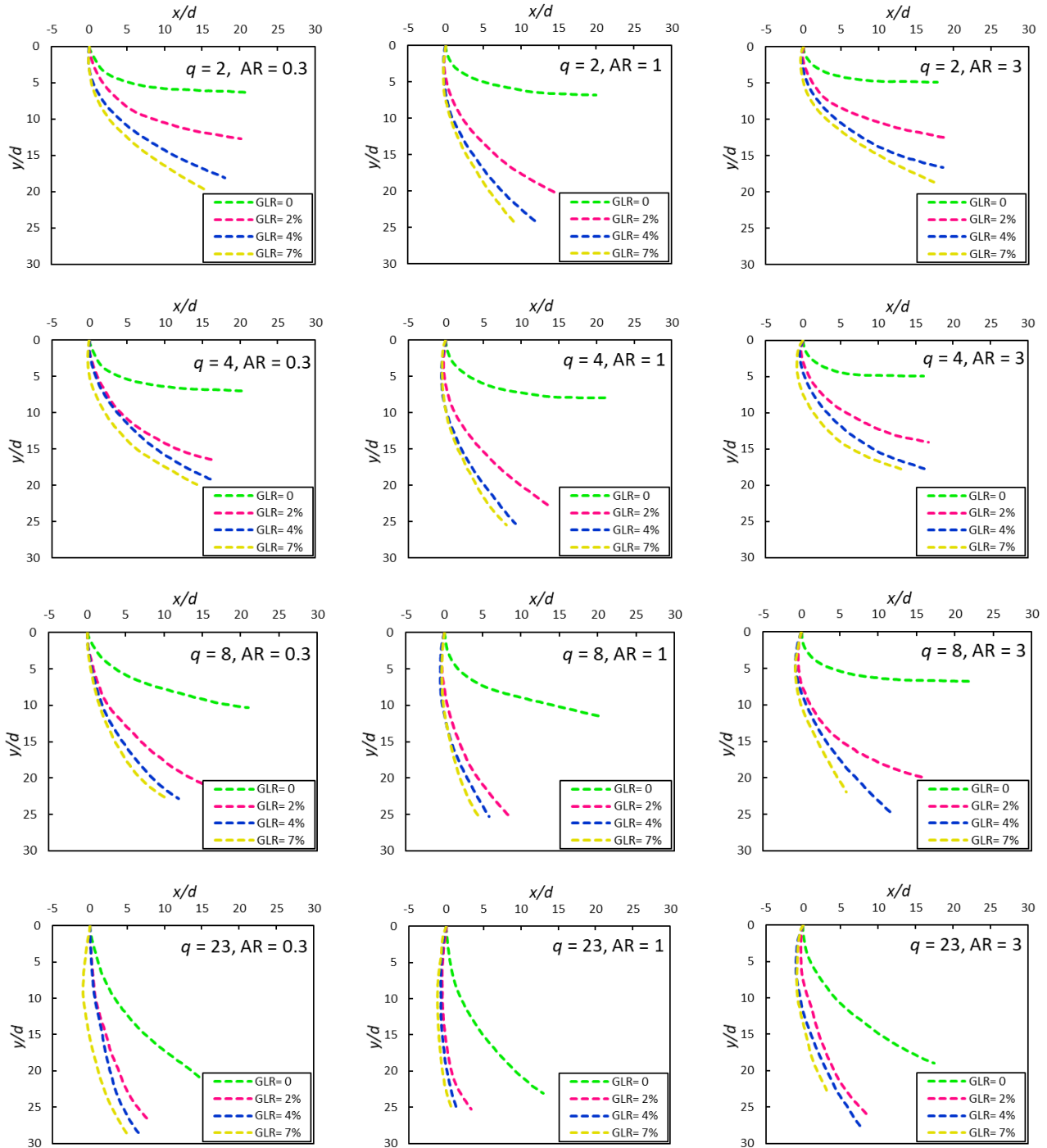
- [38] A. Saleh, G. Amini, and A. Dolatabadi, “Penetration of Aerated Suspension Spray in a Gaseous Crossflow,” *AAS*, vol. 28, no. 2, 2018, doi: 10.1615/AtomizSpr.2018019508.
- [39] J. E. Seay, V. G. McDonell, and G. S. Samuelson, “Atomization and dispersion from a radial airblast injector in a subsonic crossflow,” 1995.
- [40] Z. P. Tan, O. Bibik, D. Shcherbik, B. T. Zinn, and N. Patel, “The regimes of twin-fluid jet-in-crossflow at atmospheric and jet-engine operating conditions,” *Physics of Fluids*, vol. 30, no. 2, p. 025101, Feb. 2018, doi: 10.1063/1.5010362.
- [41] E. Farvardin and A. Dolatabadi, “Breakup Simulation of Elliptical Liquid Jet in Gaseous Crossflow,” in *42nd AIAA Fluid Dynamics Conference and Exhibit*, American Institute of Aeronautics and Astronautics.
- [42] M. R. Morad and H. Khosrobeygi, “Penetration of elliptical liquid jets in low-speed crossflow,” *Journal of Fluids Engineering*, vol. 141, no. 1, 2019.
- [43] M. Jadidi, V. Sreekumar, and A. Dolatabadi, “Breakup of elliptical liquid jets in gaseous crossflows at low Weber numbers,” *J Vis*, vol. 22, no. 2, pp. 259–271, Apr. 2019, doi: 10.1007/s12650-018-0537-8.
- [44] M. Mousavi and A. Dolatabadi, “Numerical study of the effect of gas-to-liquid ratio on the internal and external flows of effervescent atomizers,” *Transactions of the Canadian Society for Mechanical Engineering*, vol. 42, no. 4, pp. 444–456, Jun. 2018, doi: 10.1139/tcsme-2017-0125.
- [45] R. A. Wade, J. M. Weerts, J. P. Gore, and W. A. Eckerle, “Effervescent atomization at injection pressures in the MPa range,” *AAS*, vol. 9, no. 6, 1999, doi: 10.1615/AtomizSpr.v9.i6.50.
- [46] S. D. Sovani, E. Chou, P. E. Sojka, J. P. Gore, W. A. Eckerle, and J. D. Crofts, “High pressure effervescent atomization: effect of ambient pressure on spray cone angle,” *Fuel*, vol. 80, no. 3, pp. 427–435, Feb. 2001, doi: 10.1016/S0016-2361(00)00105-8.
- [47] J. G. Hong, K. W. Ku, S. R. Kim, and C.-W. Lee, “Effect of cavitation in circular nozzles and elliptical nozzles on the spray characteristic,” *AAS*, vol. 20, no. 10, 2010, doi: 10.1615/AtomizSpr.v20.i10.40.
- [48] D. W. Loebker and H. L. Empie Jr, “Effervescent spraying: a new approach to spraying high solids black liquor,” 1998.
- [49] J. Karnawat and A. Kushari, “Controlled atomization using a twin-fluid swirl atomizer,” *Exp Fluids*, vol. 41, no. 4, p. 649, Aug. 2006, doi: 10.1007/s00348-006-0191-0.

- [50] X. Huang, X. S. Wang, and G. X. Liao, "Characterization of an effervescent atomization water mist nozzle and its fire suppression tests," *Proceedings of the Combustion Institute*, vol. 33, no. 2, pp. 2573–2579, Jan. 2011, doi: 10.1016/j.proci.2010.06.001.
- [51] K.-C. Lin, P. Kennedy, and T. Jackson, "Penetration heights of liquid jets in high-speed crossflows," in *40th AIAA Aerospace Sciences Meeting & Exhibit*, American Institute of Aeronautics and Astronautics.
- [52] M. T. Lund, C. Q. Jian, P. E. Sojka, J. P. Gore, and M. V. Panchagnula, "The Influence of Atomizing Gas Molecular Weight on Low Mass Flowrate Effervescent Atomizer Performance," *Journal of Fluids Engineering*, vol. 120, no. 4, pp. 750–754, Dec. 1998, doi: 10.1115/1.2820733.
- [53] J. Li, A. H. Lefebvre, and J. R. Rollbuhler, "Effervescent Atomizers for Small Gas Turbines," in *Volume 3: Coal, Biomass and Alternative Fuels; Combustion and Fuels; Oil and Gas Applications; Cycle Innovations*, The Hague, Netherlands, Jun. 1994, p. V003T06A048, doi: 10.1115/94-GT-495.
- [54] K. Sallam, K.-C. Lin, and C. Carter, "Spray Structure of Aerated Liquid Jets Using Double-View Digital Holography," in *48th AIAA Aerospace Sciences Meeting Including the New Horizons Forum and Aerospace Exposition*, American Institute of Aeronautics and Astronautics.
- [55] M. R. Morad and H. Khosrobeygi, "Penetration of Elliptical Liquid Jets in Low-Speed Crossflow," *Journal of Fluids Engineering*, vol. 141, no. 011301, Jun. 2018, doi: 10.1115/1.4040373.
- [56] Y. Song, D. Hwang, and K. Ahn, "Effect of Orifice Geometry on Column Trajectories of Liquid Jets in Crossflows," *Int. J. Aeronaut. Space Sci.*, vol. 20, no. 1, pp. 139–149, Mar. 2019, doi: 10.1007/s42405-018-0130-3.
- [57] S. Shaghaghian, M. Jadidi, and A. Dolatabadi, "Spray Structure of an Elliptical Effervescent Atomizer," presented at the The 5th World Congress on Momentum, Heat and Mass Transfer, Oct. 2020, doi: 10.11159/icmfht20.155.
- [58] C. A. Schneider, W. S. Rasband, and K. W. Eliceiri, "NIH Image to ImageJ: 25 years of image analysis," *Nature Methods*, vol. 9, no. 7, Art. no. 7, Jul. 2012, doi: 10.1038/nmeth.2089.

# Appendix

## Appendix A

Effect of gas-liquid ratio (GLR) on the penetration height at various AR and  $q$ .



## Appendix B

Effect of liquid-air momentum flux ratio  $q$  on the penetration height at various AR and GLR %.

